iScience

CellPress
OPEN ACCESS

Article

Widespread ribosome stalling in a genome-reduced bacterium and the need for translational quality control

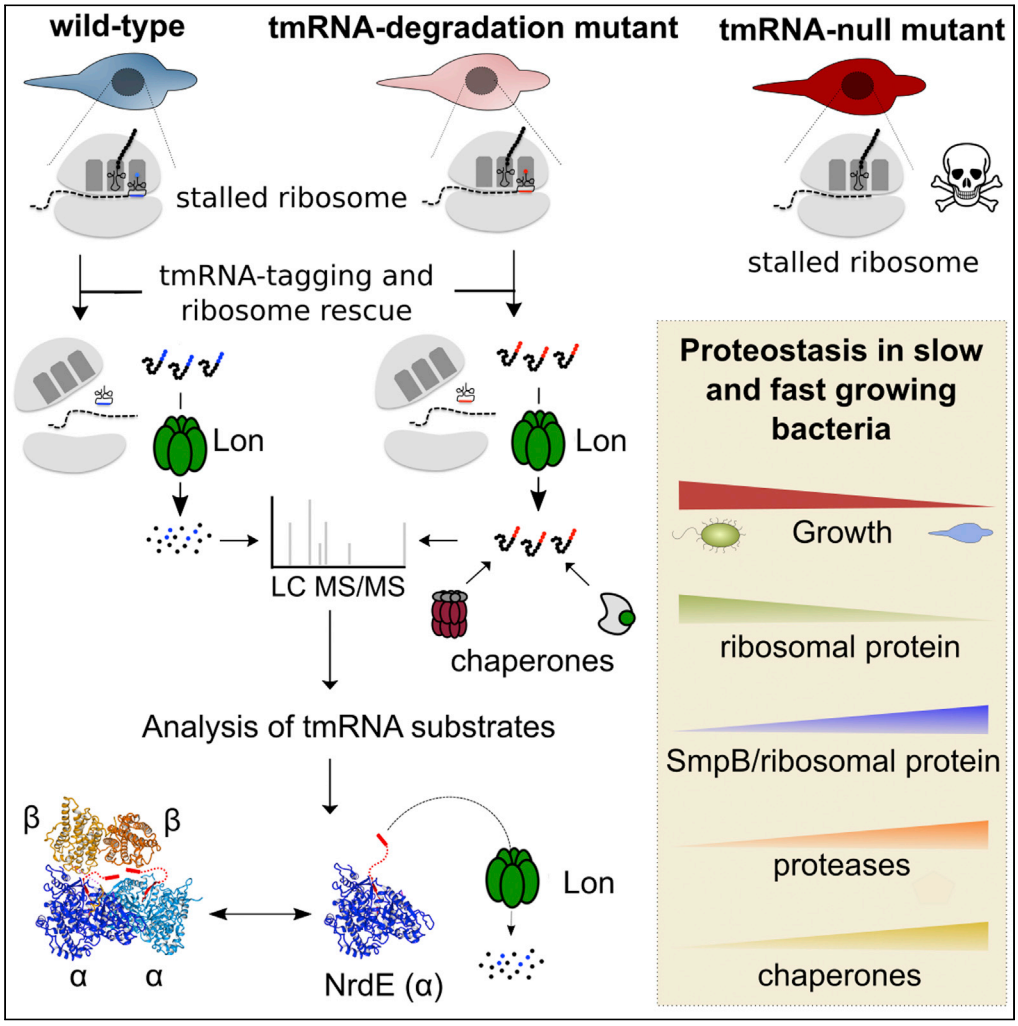

Raul Burgos, Marc Weber, Carolina Gallo, Maria Lluch-Senar, Luis Serrano

raul.burgos@crg.eu (R.B.)
luis.serrano@crg.eu (L.S.)

Highlights

Lon degrades efficiently tmRNA-tagged proteins in a genome-reduced bacterium

tmRNA-tag mutants are viable and reveal extensive tagging activity in *M. pneumoniae*

Co-evolution of Lon and their substrates offer simple mechanisms of regulation

Chaperone and Lon relative levels correlate with bacterial growth rates

Burgos et al., iScience 24, 102985
September 24, 2021
https://doi.org/10.1016/j.isci.2021.102985

iScience

CellPress
OPEN ACCESS

Article

Widespread ribosome stalling in a genome-reduced bacterium and the need for translational quality control

Raul Burgos,[1,*] Marc Weber,[1] Carolina Gallo,[1] Maria Lluch-Senar,[1] and Luis Serrano[1,2,3,4,*]

SUMMARY

Trans-translation is a ubiquitous bacterial mechanism of ribosome rescue mediated by a transfer-messenger RNA (tmRNA) that adds a degradation tag to the truncated nascent polypeptide. Here, we characterize this quality control system in a genome-reduced bacterium, *Mycoplasma pneumoniae* (MPN), and perform a comparative analysis of protein quality control components in slow and fast-growing prokaryotes. We show *in vivo* that in MPN the sole quality control cytoplasmic protease (Lon) degrades efficiently tmRNA-tagged proteins. Analysis of tmRNA-mutants encoding a tag resistant to proteolysis reveals extensive tagging activity under normal growth. Unlike knockout strains, these mutants are viable demonstrating the requirement of tmRNA-mediated ribosome recycling. Chaperone and Lon steady-state levels maintain proteostasis in these mutants suggesting a model in which co-evolution of Lon and their substrates offer simple mechanisms of regulation without specialized degradation machineries. Finally, comparative analysis shows relative increase in Lon/Chaperone levels in slow-growing bacteria suggesting physiological adaptation to growth demand.

INTRODUCTION

Protein synthesis is one of the most energetically expensive processes of an organism, having a strong impact on the growth rate of bacteria (Bosdriesz et al., 2015). It is not surprising, then, that several mechanisms have evolved at different levels to ensure proper protein production (Wickner et al., 1999; Reynolds et al., 2010). Ribosomal arrest on truncated mRNAs is one of the most severe threats to translation. This occurs when a ribosome reaches the 3'end of a truncated mRNA lacking a stop codon, which prevents translation termination and the release of the ribosome. If stalled ribosomes accumulate in the cell, the ribosome pool can be rapidly depleted, subsequently leading to cell death. To solve this problem, bacteria have evolved ribosome rescue pathways to release the nascent peptide and recover the ribosomes for further cycles of translation (Keiler, 2015; Buskirk and Green, 2017; Huter et al., 2017; Müller et al., 2021).

In bacteria, *trans-translation* is the main system for recycling ribosomes and is mediated by an RNA molecule known as transfer-messenger RNA (tmRNA), 10S RNA or small stable RNA (*ssrA*) (Janssen and Hayes, 2012). The tmRNA is structurally similar to a tRNA with capacity to be aminoacylated by alanyl-tRNA synthetases (Giudice et al., 2014). After forming a ternary complex with EF-Tu and SmpB, the tmRNA is capable of recognizing stalled ribosomes and is accommodated into the vacant A-site following EF-Tu release. Then, the nascent peptide is transferred to the tmRNA-SmpB complex being elongated with an alanine. Importantly, the translocation process to the peptidyl-tRNA binding site allows the positioning of a short open reading frame encoded by the tmRNA into the mRNA channel. This promotes the release of the non-stop mRNA, which is degraded afterward, thus preventing futile rounds of translation on the same damaged transcript (Yamamoto et al., 2003; Domingues et al., 2015). As the coding frame of tmRNA does contain a stop codon, this change of template allows both the resumption of translation and the final release of the ribosome. Notably, the coding region of tmRNA encodes a degradation tag, thus promoting the elimination of an otherwise truncated and possibly nonfunctional product. In *Escherichia coli*, the ClpXP protease assisted by the adaptor protein SspB is the principal responsible for degradation of tmRNA-tagged products (Gottesman et al., 1998; Levchenko et al., 2000).

[1]Centre for Genomic Regulation (CRG), the Barcelona Institute of Science and Technology, Dr. Aiguader 88, Barcelona 08003, Spain

[2]Universitat Pompeu Fabra (UPF), Barcelona, Spain

[3]ICREA, Pg. Lluis Companys 23, Barcelona 08010, Spain

[4]Lead contact

*Correspondence: raul.burgos@crg.eu (R.B.), luis.serrano@crg.eu (L.S.)

https://doi.org/10.1016/j.isci.2021.102985

Bacteria can initiate translation before transcription is complete and, unlike eukaryotes, they lack quality control mechanisms to assess mRNA integrity (Gallie, 1991; Doma and Parker, 2007). Therefore, the presence of truncated transcripts and henceforth ribosomal stalling can be relatively common in bacteria, especially under stress conditions (Moore and Sauer, 2005; Li et al., 2008). Truncated transcripts can be generated by premature termination of transcription, ribonuclease activity, or chemical/physical damage. Frameshifting or readthrough of stop codons can result also in translation of mRNAs lacking in-frame stop codons. Moreover, ribosome pausing can occur on intact mRNAs, generally due to the presence of rare codons, inefficient translation termination or the existence of specific stalling sequence motifs (Janssen and Hayes, 2012). In some cases, these stalling motifs are conditionally regulated and only active in certain conditions (Nakatogawa et al., 2004; Nam et al., 2016). Ribosome pausing on intact transcripts is generally resolved, but if stalling persists, the mRNA can be cleaved in the A-site generating a non-stop translation complex that is eventually targeted by a ribosome rescue system (Hayes and Sauer, 2003).

The tmRNA-SmpB system is conserved throughout the bacterial kingdom, highlighting its fundamental role. Generally, only in those species with backup systems such as ArfA, ArfB, ArfT, or BrfA, the *tmRNA,* and *smpB* genes are dispensable, as occurs for example in *E. coli*, *Caulobacter crescentus, Francisella tularensis,* or *Bacillus subtilis* (Chadani et al., 2010; Feaga et al., 2014; Goralski et al., 2018; Shimokawa-Chiba et al., 2019). Inactivation of trans-translation results in different phenotypic responses, often making cells less resistant to stressful conditions (Janssen and Hayes, 2012). In certain species, however, trans-translation also plays a regulatory role in controlling specific cellular events (Barends et al., 2011).

In this study, we investigated the role of tmRNA in the model organism *Mycoplasma pneumoniae*, a respiratory human pathogen characterized by a minimal genome. This bacterium has a reduced set of proteases, lacking ClpXP and obvious protein adaptors (Burgos et al., 2020). In addition, essentiality studies suggest it relies solely upon the tmRNA pathway for releasing stalled ribosomes (Lluch-Senar et al., 2015). While the tmRNA sequence is highly conserved across bacteria, *M. pneumoniae* encodes an unusual long degradation tag comprising 27 amino acids, as compared with the 11 and 14 residues of the *E. coli* and *B. subtilis* tags. *In vitro* studies using recombinant proteins have suggested that the mycoplasma tag has evolved to facilitate recognition by the Lon protease (Gur and Sauer, 2008; Ge and Wali Karzai, 2009), but this has not been directly demonstrated in mycoplasma cells. Here, we first performed a quantitative analysis of protein quality control components combined with a comparative analysis in slow and fast-growing bacteria, underscoring cellular proteostasis adaptation to different growth rates. Then, we examined the activity of the tmRNA system in *M. pneumoniae* by combining genetic and high-throughput proteomic approaches. We demonstrated that the essentiality of the tmRNA system is due to its role in releasing ribosomes rather than its role in marking proteins for degradation. We also showed that Lon is the main protease degrading tmRNA-tagged products *in vivo*. To understand the extent of tmRNA activity across the proteome, we performed a proteome wide analysis of tmRNA substrates. Interestingly, NrdE was identified as one of the major targets of tmRNA activity, producing stable subunits lacking the C-terminal cysteine pair required for the regeneration of the ribonucleotide reductase (RNR) catalysis. Further analysis also showed that the C-terminal region of NrdE serves as a Lon-degradation signal, suggesting an underlying mechanism by which RNR complex formation is dynamically regulated by Lon-dependent degradation.

RESULTS

Relative abundances of protein quality control components are increased in slow-growing bacteria

M. pneumoniae is a slow-growing (divides every 8 hr) bacterium possessing only about 200-300 ribosomes per cell (Seybert et al., 2006; Maier et al., 2011). Quantitative analysis of components of the trans-translation machinery of *M. pneumoniae* reveals about 24 protein copies of SmpB (MPN074) and 19 copies of the tmRNA (MPNs04), suggesting the existence of approximately one tmRNA system for every 10 ribosomes. To examine whether this capacity of trans-translation is similar in other bacteria containing higher ribosome content, we performed a comparative study across slow- and fast-growing bacteria (Figure 1). For this, we included in the analysis 7 species of mycoplasma that like *M. pneumoniae* lack alternative ribosome rescue systems and exhibit cell doubling times ranging between 0.5 hr (*M. feriruminatoris*) to 16 hr (*M. genitalium*). We found that the ribosomal protein content negatively correlated with the cell doubling time, suggesting higher abundance of ribosomes in fast-growing bacteria (Figure 1A). This trend was previously described in *E. coli* that is approximately 10 times larger in volume than *M. pneumoniae* and contains between 8,000

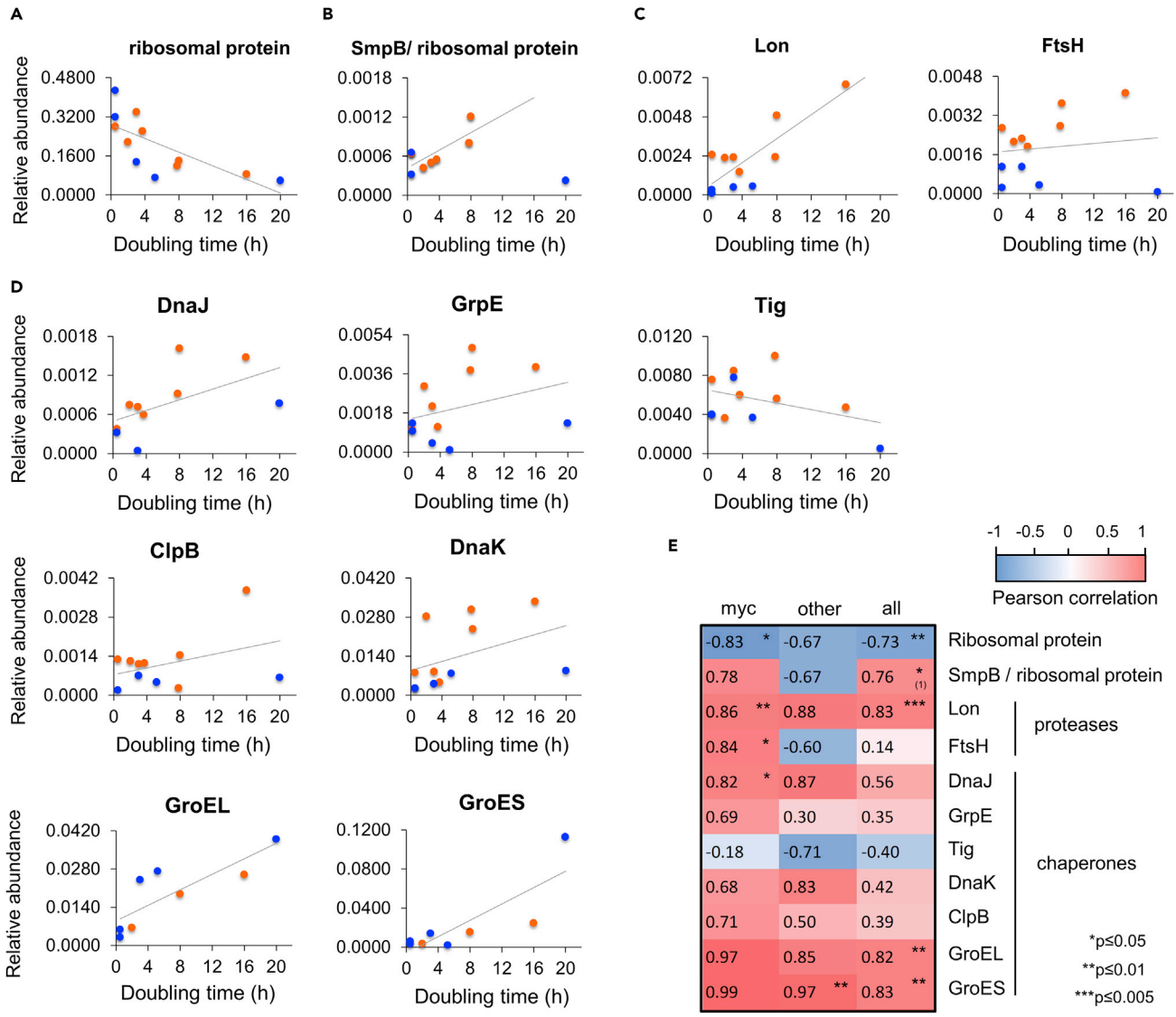

Figure 1. Relative abundances of protein quality control components correlate with growth rate

(A–D) Relative protein abundances of quality control components are shown for several bacterial species exhibiting different doubling times. Orange dots represent protein relative abundances when detected for 7 different mycoplasma species, including *M. genitalium*, *M. pneumoniae*, *M. hyopneumoniae*, *M. capricolum*, *M. mycoides*, *M. gallisepticum* and *M. feriruminatoris*. Blue dots represent data for other bacterial species including *M. tuberculosis*, *D. vulgaris*, *C. jejuni*, *B. subtilis* and *E. coli*. Correlation plots show relative abundances of (A) ribosomal proteins (considering approximately 52 ribosomal proteins per each bacterial species), (B) SmpB abundance relative to ribosomal content (the line trend presented excludes *M. tuberculosis*), (C) ATP-dependent proteases found in mycoplasmas, and (D) major chaperone systems.

(E) Pearson correlation matrix and statistical analysis for mycoplasma species only (myc), other bacterial species only (other), or considering all species analyzed (all). (1) Pearson correlation for SmpB/ribosomal protein ratio does not include *M. tuberculosis* when considering all bacterial species.

See also Figures S1 and S2.

(at 0.6 doubling per hour) and 73,000 (at 3 doubling per hour) ribosomes per cell (Bremer and Dennis, 2008). When comparing the SmpB abundance relative to the ribosomal protein content, we observed the opposite trend, suggesting a slightly higher trans-translation capacity in slow-growing bacteria (Figure 1B). SmpB and/or tmRNA levels may vary in response to environmental perturbations as shown for example in mycobacteria after exposing cells to ribosome inhibitors (Andini and Nash, 2011). This, and the unusual fact that SmpB is not essential in *Mycobacterium tuberculosis* (Personne and Parish, 2014) may explain why this particular pathogen seems an exception with regard to the observed correlation trend (Figure 1B). In the case of *M. pneumoniae*, we did not observe significant changes in expression of *tmRNA* and *smpB*

genes upon different perturbations analyzed (Figure S1) (Yus et al., 2019), yet we found *tmRNA* up-regulation (1.9 log_2) after depletion of Lon. This particular transcriptional response may be related to the fact that Lon depletion results in down-regulation of ribosomal proteins (Burgos et al., 2020).

Since the tmRNA system works in concert with other protein quality control systems, we also compared the relative abundances of chaperone and proteases across slow and fast-growing bacteria. In mycoplasma species where Lon is the sole cytoplasmic ATPase dependent protease, we found that its relative expression levels were significantly higher in slow dividing species (Figures 1C and 1E). A similar trend is observed for other bacteria, yet in these species additional proteases may complement Lon function. Regarding the membrane-anchored FtsH protease we also observed a slight correlation with the doubling time in mycoplasma, but this trend was not observed for the other bacterial species analyzed (Figures 1C and 1E). Interestingly, we found that the relative levels of different chaperones were also increased in slow-growing bacteria, except for the trigger factor (Figures 1D and 1E). This trend was particularly significant for the GroEL/ES chaperon system, which was observed for the majority of bacterial species analyzed. The distribution of Pearson correlation coefficients considering all proteins with an ortholog detected by MS in at least 4 mycoplasma species (338 proteins) showed no specific enrichment toward positive or negative correlation coefficients (binomial test, $p = 0.48$, see Figure S2). Overall, these results show that chaperone and Lon relative abundances correlate well with the cell doubling time, suggesting a physiological adaptation to maintain proteostasis in response to the growth rate demand.

M. pneumoniae ssrA-tag promotes efficient Lon-mediated protein degradation *in vivo*

To characterize the tmRNA system of *M. pneumoniae*, we first examined whether the unusual degradation tag encoded by the *ssrA* gene (MPNs04) is efficiently recognized *in vivo* by the protease set encoded by this organism. For this, we fused the ssrA-tag at the C-terminus of the chloramphenicol acetyltransferase (*cat*) gene reporter (cat_TssrA), and we assessed its expression in wild-type cells by Western blot and chloramphenicol survival assays. In these experiments, we did not detect the CAT_TssrA fusion using anti-CAT antibodies, or chloramphenicol resistance among the transformed cells (Figure S3), a result consistent with tag-mediated degradation of the CAT reporter. We then assessed the contribution to this targeted proteolysis of the two ATP-dependent proteases present in *M. pneumoniae*: Lon and FtsH. Since both proteases are essential for growth in *M. pneumoniae*, we expressed the CAT_TssrA fusion in conditional mutants, in which Lon and FtsH expression is under the control of a Tet-inducible promoter (Burgos et al., 2020). Since these mutants were engineered and selected with the *cat* resistance selectable marker, we detected as expected the CAT untagged protein in both mutants when using anti-CAT antibodies (Figure 2A). Interestingly, we also detected a band corresponding to the tagged form of CAT (CAT_TssrA) but only after shutting down the expression of Lon (Figure 2A). This band was not detected under FtsH depleting conditions, suggesting that Lon plays a major role in the degradation of tmRNA-tagged proteins in *M. pneumoniae*. Supporting these observations, we obtained similar results when using polyclonal antibodies raised against the ssrAmk-tag (see STAR Methods). In this case, we only detected the tagged form of CAT as expected, and only under Lon depleting conditions (Figure 2A). These results indicate that polyclonal antibodies raised against the mutant ssrAmk-tag (see below) recognize epitopes also present in the wild-type sequence tag. Consistently, when whole-cell lysates of Lon or FtsH depleted cells were probed with anti-ssrAmk tag antibodies, we could distinguish multiple reacting proteins of different molecular sizes in the absence of Lon (Figure 2B). This observation is consistent with the accumulation of multiple endogenous ssrA-tagged proteins, indicating that the ssrA-tag of *M. pneumoniae* is acting as an efficient degradation signal for Lon-mediated degradation *in vivo*.

Protein degradation targeted by tmRNA is not essential for M. pneumoniae cell growth

To assess tmRNA activity *in vivo*, we constructed an *ssrA* mutant in *M. pneumoniae* capable of inducing tagging with an ssrA-tag resistant to proteolysis. For this, we modified the *ssrA* gene by replacing the tag codons encoding NYA by aspartic acid codons (Figure 3A). This mutation strategy was based on a previous study, in which similar amino acid substitutions were shown to prevent tag-mediated degradation in *in vitro* assays (Ge and Wali Karzai, 2009). To facilitate later MS analyses after trypsin digestion, we also mutated the lysine and glutamic acid residues found in the third and seventh position of the tag by aspartic acid and lysine, respectively (Figure 3A). RNA folding analyses predicted that these mutations did not impact the overall structure of the tmRNA molecule (Figure S4). Then, we verified how these mutations affected ssrA tag-mediated protein degradation *in vivo*. Using CAT reporter fusions, we found that unlike the ssrA wild-type tag, addition of the mutated tag (herein referred as ssrAmk) resulted in detectable

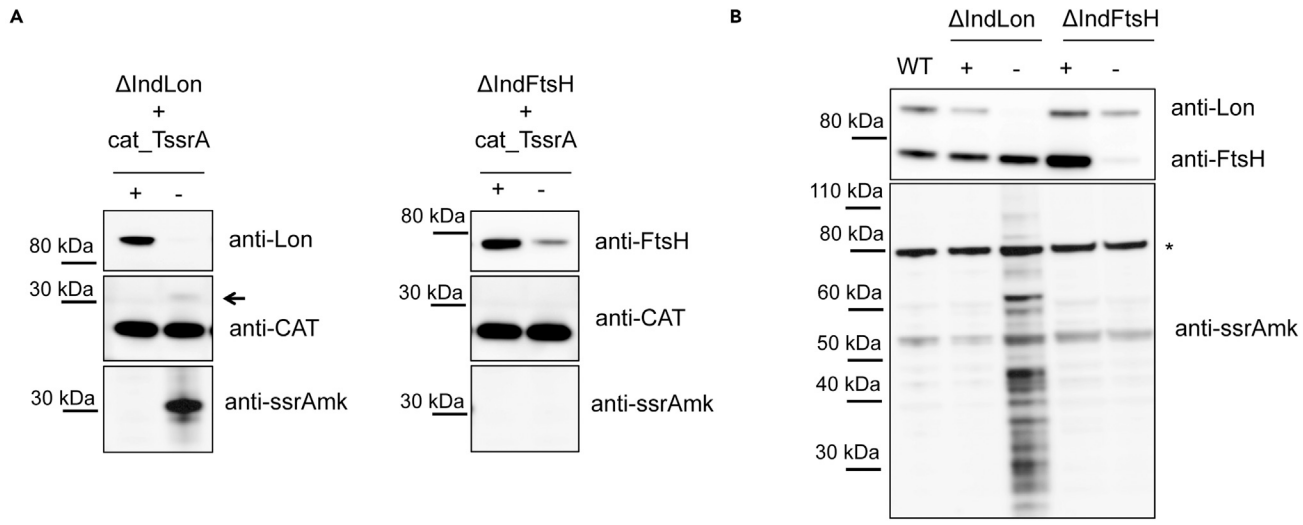

Figure 2. The ssrA-tag of *M. pneumoniae* acts as a degradation signal for Lon-mediated degradation

(A) ΔIndLon and ΔIndFtsH mutant strains expressing a CAT reporter protein fused to the wild-type ssrA-tag (TssrA) were grown under inducing (+) or depleting (–) conditions. Expression of the CAT-tagged variant was then assessed by Western blot analysis using anti-CAT and anti-ssrAmk antibodies. Note that ΔIndLon and ΔIndFtsH mutant strains also express the wild-type CAT resistance marker, which was used for selecting the transformants during the engineering process. An arrow indicates the CAT-tagged variant. Anti-Lon and anti-FtsH antibodies were used to evaluate the level of protease depletion in each condition.

(B) Role of Lon and FtsH in degrading endogenous ssrA-tagged proteins. ΔIndLon and ΔIndFtsH mutant strains were grown under inducing (+) or depleting (–) conditions. Then, the level of ssrA-tagged endogenous proteins present in each condition was assessed by Western blot analysis using anti-ssrAmk antibodies. Anti-Lon and anti-FtsH antibodies were used to evaluate the level of protease depletion in each condition. Asterisk shows unspecific bands that serve as loading controls.

See also Figure S3.

expression of the CAT reporter, using both anti-CAT and anti-ssrAmk tag antibodies (Figure 3A). In fact, we confirmed that only those mutations in the C-terminal residues of the tag protected the reporter protein from being degraded *in vivo*, conferring chloramphenicol resistance to transformed cells (Figure S3). We also found that addition of the ssrAmk-tag caused a decrease in the levels of CAT as compared with the untagged variant (Figure 3A). This reduction in expression could be explained either by interference of the tag with translation and protein folding of CAT, or incomplete degradation inhibition.

To test the functionality of the *ssrA* mutant gene encoding the ssrAmk-tag, whole cell lysates of wild-type cells expressing the mutant gene variant were assessed by Western blot (Figure 3B). Purified antibodies raised against the mutant ssrAmk tag reacted with multiple proteins of different molecular sizes, revealing extensive tagging across the proteome. Very little reactivity was observed on samples expressing the wild-type *ssrA* gene that encodes a functional degradation tag (Figure 3B), thus confirming the specificity of the sequence recognized by the antibody. Additional analyses of tagging activity along the growth curve showed that signal intensity increased progressively, suggesting either accumulation of ssrA-tagged proteins over time or increased tmRNA activity when approaching the stationary growth phase (Figure S5). Of note, we failed to detect tagging activity when the *ssrAmk* gene was expressed from a P438 constitutive promoter (Pich et al., 2006), suggesting that the 5′UTR of *ssrA* is required for *ssrA* function (Figure S6). This interpretation is consistent with the fact that the *ssrA* gene is synthetized initially as a precursor and needs to be processed into a mature form (Komine et al., 1994).

Transposon essentiality studies in *M. pneumoniae* have shown that the *ssrA* gene is essential for cell growth (Lluch-Senar et al., 2015). To further characterize this essentiality, we deleted the endogenous *ssrA* gene in a mutant background expressing the *ssrAmk* variant (Figure 3B). The fact that we succeed in performing this deletion indicates that the *ssrAmk* variant can complement the essential functions of the *ssrA* endogenous gene (Figure S7). Western blot analyses of cell extracts derived from this deletion mutant showed a similar tagging pattern compared with the wild-type strain expressing the *ssrAmk* variant but with a much more intense signal (Figure 3B). This observation suggests that although tmRNA activity is extensive, its capacity is not overwhelmed under normal growth conditions. To further examine how the accumulation of tagged

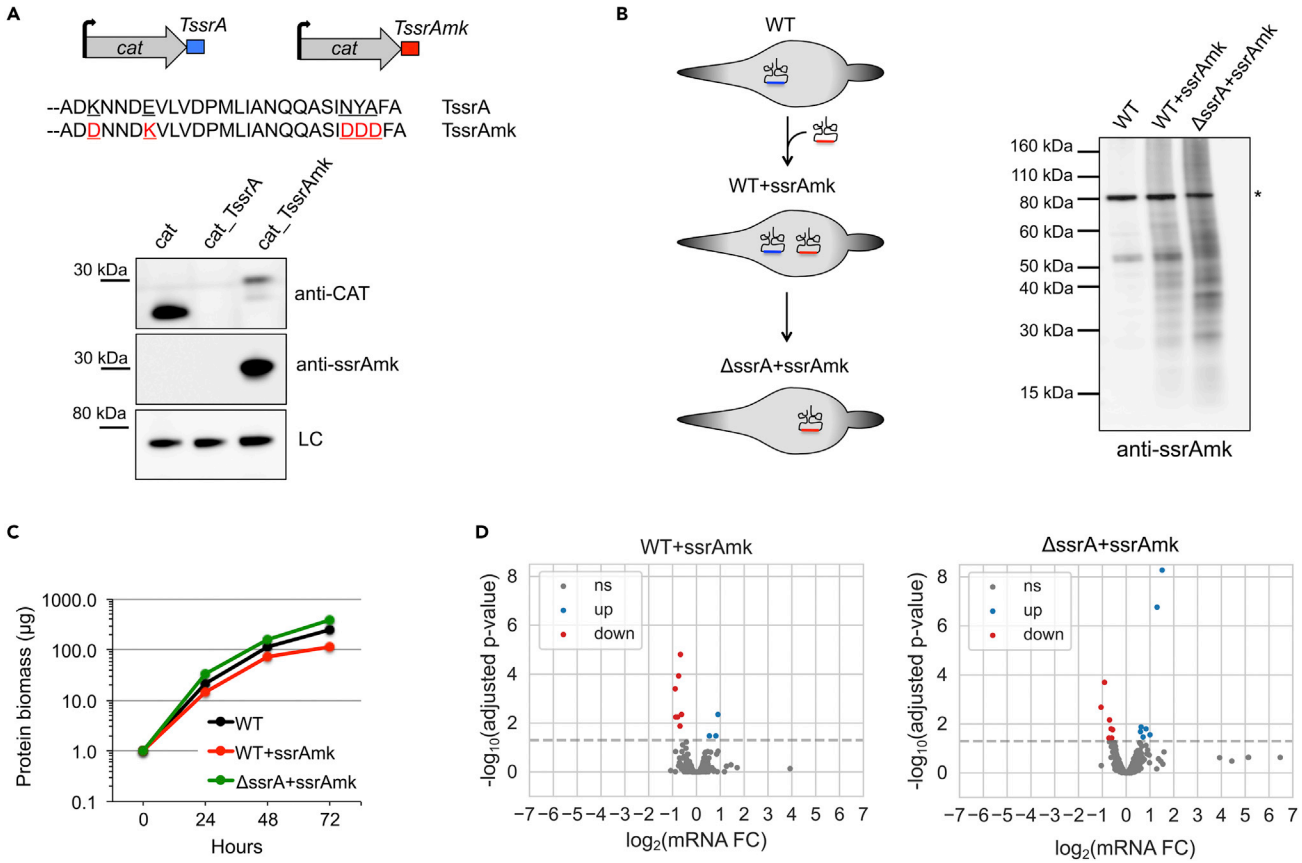

Figure 3. Construction and analysis of *ssrA* mutant variants of *M. pneumoniae* encoding a ssrA-tag resistant to proteolysis

(A) Amino acid sequence of wild-type ssrA-tag (TssrA) and a tag variant (TssrAmk) resistant to proteolysis. Residues mutated are highlighted in red. Below, Western blot analysis using anti-CAT and anti-ssrAmk antibodies assessing the stability in wild-type cells of the CAT reporter protein and CAT fusions to TssrA or TssrAmk tags. LC, loading control.

(B) Schematic representation of the construction of *ssrA* mutant variants of *M. pneumoniae* encoding a ssrA-tag resistant to proteolysis. Briefly, the *ssrAmk* gene variant (in red) encoding the TssrAmk tag was introduced in the wild-type (WT) strain to obtain the WT + ssrAmk mutant. Then, the endogenous *ssrA* gene (in blue) was deleted obtaining the ΔssrA + ssrAmk strain. Functionality of the *ssrAmk* gene variant was assessed by Western blot analysis using anti-ssrAmk antibodies, revealing the presence of numerous stable ssrAmk-tagged proteins. Asterisk shows unspecific bands that serve as loading controls.

(C) Growth curve analyses determined by protein biomass measurements of WT, WT + ssrAmk and ΔssrA + ssrAmk mutant strains. The average of two independent biological replicates is shown.

(D) Volcano plot of statistical significance against transcriptional changes upon expression of the *ssrAmk* gene variant, in the WT (left) and ΔssrA (right) genetic backgrounds. Significantly up-regulated (up) genes are shown in blue, significantly down-regulated (down) genes are shown in red, genes not significantly differentially expressed (ns) at a false discovery rate of 5% (dashed horizontal line) are shown in grey. Data represent the average of two independent clones per strain and assayed per duplicate.

See also Figures S4–S7 and Table S1.

proteins may affect growth, we performed growth curve analyses of the two mutant strains expressing the *ssrAmk* gene variant (with or without the endogenous *ssrA* gene). Both mutant strains exhibited similar growth rates as compared with the wild-type strain (Figure 3C). These results suggest that *M. pneumoniae* is capable to cope with a certain degree of truncated proteins, yet we cannot discard that toxic effects may appear if these products over-accumulate after consecutive passages. In line with this, very few transcriptional changes were observed following *ssrAmk* gene expression (Figure 3D, Table S1). In fact, of 757 genes only 3 and 7 were found significantly up- and downregulated in the wild-type strain expressing the *ssrAmk* variant, whereas 7 genes were up- or downregulated in the strain with the deleted endogenous *ssrA* gene. Of note, no overlap was found between both strains, and only 4 genes exhibited fold changes higher than ±1-fold (log_2). These results support the notion that the level of tagged proteins accumulated in these mutants is within the physiological acceptable limits. Thus, we conclude that the tagging activity of the *ssrA* gene in delivering proteins for degradation has a minor contribution in the

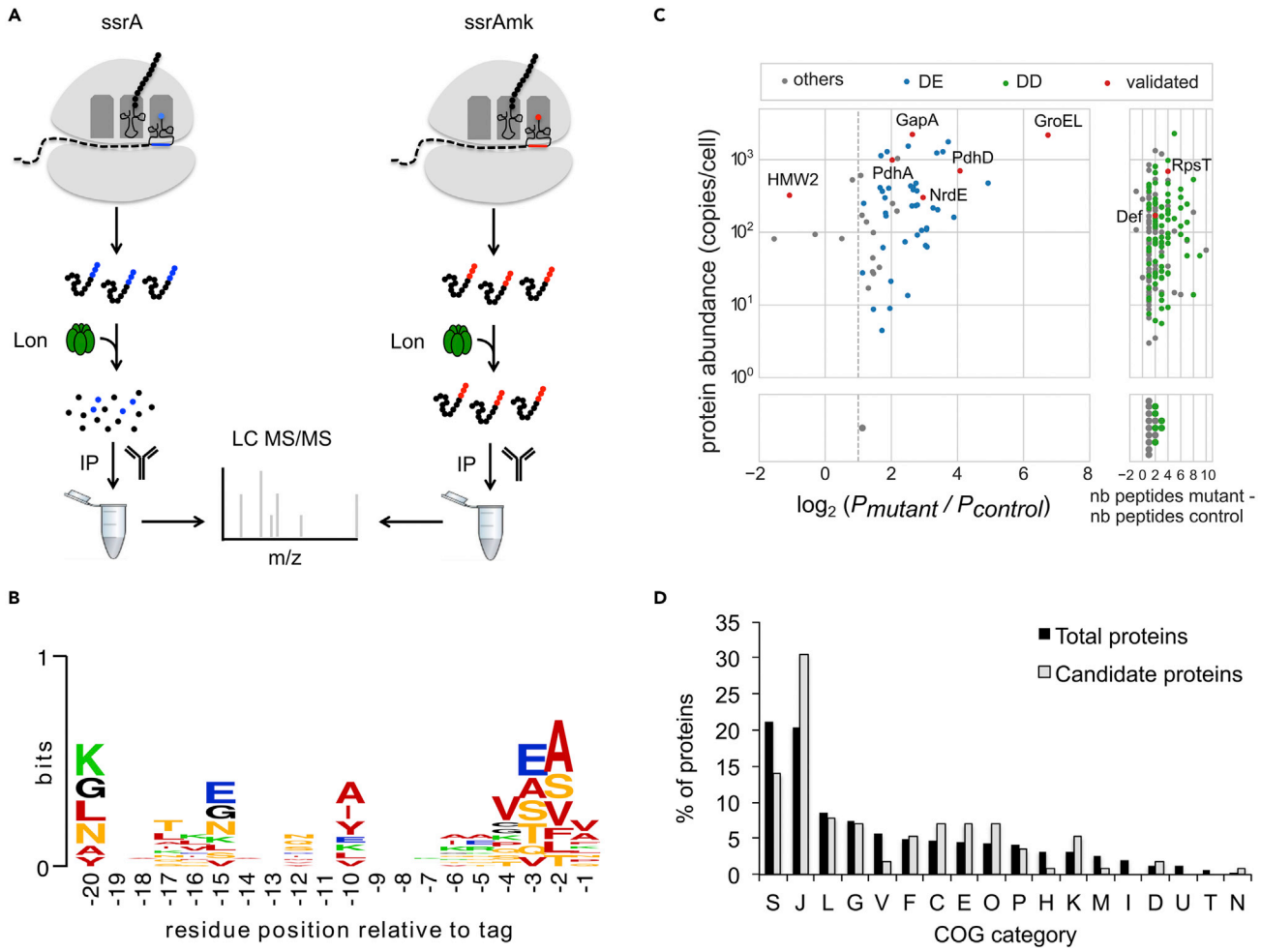

Figure 4. Identification and analysis of tmRNA substrates

(A) Illustration of the workflow strategy to identify tmRNA substrates.

(B) Weblogo analysis of the amino acid sequences preceding the tmRNA tagging sites. Hydrophobic amino acids are shown in red, uncharged polar amino acids in orange, positively charged amino acids in green, negatively charged amino acids in blue and other amino acids in black.

(C) Enrichment plot of proteins detected under IP stringent conditions vs. protein copy number per cell (Maier et al., 2011). Horizontal axis shows $\log_2$ of the fold change in protein abundance between mutant (*Pmutant*) and control (*Pcontrol*) IP samples (left panel), or difference in the number of peptides detected (right panel). In blue are shown putative tmRNA substrates differentially enriched (DE) by > 1 $\log_2$ in the two mutant IP samples (P_{mutant}). In green are shown candidate substrates differentially detected (DD) in the two mutant IP samples but not detected in control. In red are indicated those tmRNA substrates for which tagged peptides were identified (validated). Detected proteins that do not meet any of the criteria are shown in gray (others). For DD proteins the number of peptides detected are shown instead of the fold change.

(D) Functional COG classification of putative tmRNA candidate substrates compared to total proteins. The Y axis represents the percentage of proteins in each COG category.

See also Table S2.

essentiality of the *ssrA* gene under normal growth conditions, and that the essential nature of the *ssrA* gene seems to be associated with its role in recovering stalled ribosomes.

Identification of tmRNA-tagged proteins in M. pneumoniae

Next, we performed a proteomic analysis to identify which proteins are tagged by tmRNA during normal growth conditions (Figure 4A). For this, we performed immunoprecipitation (IP) assays using the anti-ssrAmk-tag antibody mentioned above and cell lysates from control and cells expressing the *ssrAmk* gene variant. Protein samples were then digested with trypsin and subjected to LC-MS/MS analyses. To identify tmRNA-tagged substrates and determine the tagging sites, we searched for peptides containing

Table 1. Protein substrates of tmRNA in *M. pneumoniae* for which tagged peptides were identified

Protein	Function	Tagged peptide sequence[a,b]	Tag[c] position	FC[d]
MPN245	Peptide deformylase (Def)	VINPALPADDNNDK[a]	189 [193]	NA
MPN310	Cytadherence-related protein (HMW2)	KEAVADDNNDK[b]	1351 [1818]	-1.08
MPN324	Ribonucleotide reductase subunit α (NrdE)	VRQEVLADDNNDK[a,b]	703 [721]	2.96
MPN324	Ribonucleotide reductase subunit α (NrdE)	VRQEVLEADDNNDK[a,b]	704 [721]	2.96
MPN324	Ribonucleotide reductase subunit α (NrdE)	VRQEVLEDADDNNDK[a,b]	705 [721]	2.96
MPN324	Ribonucleotide reductase subunit α (NrdE)	VRQEVLEDSEDADDNNDK[a]	708 [721]	2.96
MPN324	Ribonucleotide reductase subunit α (NrdE)	VRQEVLEDSEDHTIQADDNNDK[a]	712 [721]	2.96
MPN324	Ribonucleotide reductase subunit α (NrdE)	VRQEVLEDSEDHTIQMQQADDNNDK[a]	715 [721]	2.96
MPN390	Dihydrolipoyl-dehydrogenase (PdhD)	HAQDYGISINGQVALNWNQLLEQKG KVVSKADDNNDK[a]	92 [457]	4.08
MPN393	Pyruvate dehydrogenase subunit α (PdhA)	IEQEVQAAADDNNDK[b]	318 [358]	2.03
MPN430	Glyceraldehyde-3-phosphate dehydrogenase (GapA)	AASASFADDNNDK[a]	274 [337]	2.64
MPN430	Glyceraldehyde-3-phosphate dehydrogenase (GapA)	IISAASCTTNADDNNDK[b]	160 [337]	2.64
MPN541	30S ribosomal protein S20 (RpsT)	TQVTAVADDNNDK[a]	84 [87]	NA
MPN573	60 kDa chaperonin (GroEL)	AASVASSLITTSVAADDNNDK[a]	529 [543]	6.74
MPN573	60 kDa chaperonin (GroEL)	EGSFQADDNNDK[a,b]	542 [543]	6.74
MPN603	ATP synthase subunit c (AtpE)	AVEAVADDNNDK[a]	64 [105]	ND

[a]Tagged peptides identified by Mascot database search.
[b]Tagged peptides identified by de novo sequencing using PEAKS software.
[c]In brackets, the position of the last residue of the protein.
[d]Protein fold change (log_2) enrichment in the mutant IP sample compared to the control sample under IP stringent conditions. NA indicates that the protein was not detected in the control IP sample. ND indicates that the protein was not detected in any of the IP samples.

both protein and tag sequences. For this, we used two complementary approaches: *de novo* peptide sequencing, and protein identification using the Mascot search engine against a database containing all possible tagged proteins. We obtained a higher recovery rate of tagged peptides with the Mascot search engine (Table 1). This could be explained because *de novo* search engines are prone to sequencing errors and might not be able to sufficiently resolve long sequences or peptides above 12–15 residues (Muth and Renard, 2018), which are in the range of the minimum size to unambiguously assign a tmRNA-tagged-peptide. In total, we identified 16 tagged peptides that passed our quality control criteria (see STAR Methods) and for which its protein sequence could be unambiguously assigned to a unique protein (Table 1). Importantly, these peptides were only found in the *ssrAmk* mutant IP samples. The tagged peptides identified derived from 9 different proteins, indicating that some substrates were tagged in several sites. Among the tmRNA substrates, half of them were involved in energy and nucleotide metabolism, including NrdE (Ribonucleotide reductase subunit α), dihydrolipoyl-dehydrogenase, pyruvate dehydrogenase subunit α, glyceraldehyde-3-phosphate dehydrogenase, and ATP synthase subunit c (AtpE). We also identified tagged peptides of Def (peptide deformylase), HMW2 (cytadherence-related protein), RpsT (30S ribosomal protein S20), and GroEL (chaperone). The tag insertion site was located near the C-terminus for the majority of substrates (Table 1). Further analysis of the DNA and amino acid sequences upstream and downstream the tagging sites did not reveal conserved sequence motifs. We did note, however, that hydrophobic and polar uncharged amino acids tend to be enriched within the last residues preceding the tagging site (Figure 4B). In fact, we detected four additional tagged peptides that could not be assigned to a unique protein but all contained hydrophobic amino acids before the tag sequence (IIV-tag, II-tag, ALF-tag, and YF-tag). However, this trend did not reach statistical significance, probably because of the limited number of tagged sites detected.

Considering that other tagged peptides may not be identified due to unfavored length after trypsin digestion, low expression, and/or low ionization efficiency, we further analyzed which proteins were enriched in the mutant compared with control IP samples, irrespective of finding the tag sequence. For this particular analysis, we used stringent IP conditions, revealing a total of 92 proteins detected only in the mutant IP samples (differentially detected, DD), and 44 proteins enriched more than 2-fold in both mutant IP samples

(differentially enriched, DE) (Figure 4C, Table S2). When using a more aggressive cut off of 1% FDR, we detected a total of 77 DD and 41 DE proteins (see Table S2). The proteins for which tagged peptides were identified were also enriched in the mutant IP samples, except HMW2 and AtpE. The latter was not detected in any of the IP samples obtained under stringent conditions, whereas the levels of HMW2 were reduced 2-fold in the mutant IP samples (Table 1 and Figure 4C). This reduction in HMW2 is likely a direct result of the insertion of the transposon used to deliver the *ssrAmk* gene variant, which was located in the upstream gene *mpn309* (P65). A similar phenotype was previously reported for other P65 transposon mutants (Hasselbring et al., 2012).

A COG enrichment analysis of the proteins enriched after immunoprecipitation did not reveal any significant association with a specific functional pathway, although proteins related to translation were mainly represented (Figure 4D). The lack of significant results of this functional enrichment analysis could be partially due to the relatively small number of genes in this bacterium. However, we found enrichment of the two major proteases of *M. pneumoniae*, Lon and FtsH; and almost the full set of chaperones, including Tig, ClpB, DnaK, GroEL/ES, and DnaJ. These observations suggest that incomplete tagged proteins form stable complexes with chaperones and proteases, yet we cannot discard that these protein quality control components may be directly tagged such in the case of GroEL.

NrdE is frequently tagged by the tmRNA system generating stable C-terminal truncated variants in M. pneumoniae

The above analysis revealed that NrdE is one of the major tmRNA targets during standard growth conditions. Intriguingly, we detected 6 distinct tagging sites, all close to the C-terminal end (Figure 5A, Table 1). Structural data indicate that tmRNA tagging in these positions would generate truncated variants with the ssrA-tag replacing the mobile C-terminal tail of NrdE. This C-terminal region of NrdE is key for its activity, as it contains a cysteine pair (CXXC) that functions as a reducing agent of the active site (Figure 5B). To investigate further this finding, we expressed an N-terminal strep-tag fusion of NrdE in cells containing the *ssrAmk* gene variant. Strep-tagged NrdE proteins were then isolated by affinity purification and tmRNA tagging analyzed by immunoblot analysis using anti-ssrAmk tag antibodies (Figure 5C). Consistent with the LC-MS/MS results, we detected NrdE tagged products with molecular weights similar to the full-length protein, indicating that tmRNA tagging is especially frequent near the C-terminal. To our surprise, we also detected similar tmRNA-tagged products when NrdE was purified from wild-type cell extracts, yet with a lower intensity (Figure 5C). This observation suggests that truncated forms of NrdE could be stable even carrying a degradation tag. To test this possibility, we generated several N-terminal FLAG derivatives of NrdE and assessed their stability in wild-type cells (Figure 5D). As expected, full-length NrdE was detected using anti-FLAG antibodies, but not when the ssrA-tag was fused to the last amino acid of NrdE, consistent with tag-mediated degradation. When the proteolysis resistant tag variant (ssrAmk) was attached instead, NrdE was detected using both anti-FLAG and anti-ssrAmk antibodies. Interestingly, in this case, we detected a stronger signal compared to the untagged form of NrdE, suggesting that addition of the ssrAmk-tag improved the protein half-life of NrdE. We also assessed the stability of one of the NrdE-tagged variants detected in our MS analysis, by adding both wild-type and mutant ssrA-tags after residue 705 (Figure 5D). Addition of the wild-type ssrA-tag did not result in full degradation of the truncated variant, indicating that the ssrA-tag may not be fully accessible in this protein form. As for the full-length NrdE, the ssrAmk-tag fusion improved stability. Altogether, these results show that the tmRNA system of *M. pneumoniae* is capable of generating stable C-terminal truncated variants of NrdE.

The C-terminal region of NrdE functions as a Lon degron

Other orthologs of NrdE have not been reported so far to be tagged by the tmRNA system, perhaps representing a specific trait across mycoplasma species. Although sequence conservation among NrdE orthologs is high, *M. pneumoniae* contains a small extended non-conserved region at the C-terminus just before the cysteine pair, which coincides with the tagged region (Figure S8). To examine the contribution of the C-terminal region of NrdE to tmRNA tagging, we constructed N-terminal strep-tagged variants of mCherry containing C-terminal fusions to the last 25 or 50 amino acids of NrdE (Figure 6A). Unlike a control mCherry variant lacking the C-terminal NrdE region, both fusion proteins could not be expressed in cells containing the *ssrAmk* gene variant (Figure 6B). Since the C-terminal region of NrdE is relatively hydrophobic, we hypothesize that it might contain Lon-degradation signals promoting turnover of the fused protein (Burgos et al., 2020). To test this possibility, we expressed the two mCherry fusion constructs in a Lon conditional mutant and assessed their stability under inducing or Lon depleting conditions (Figure 6C). Consistent

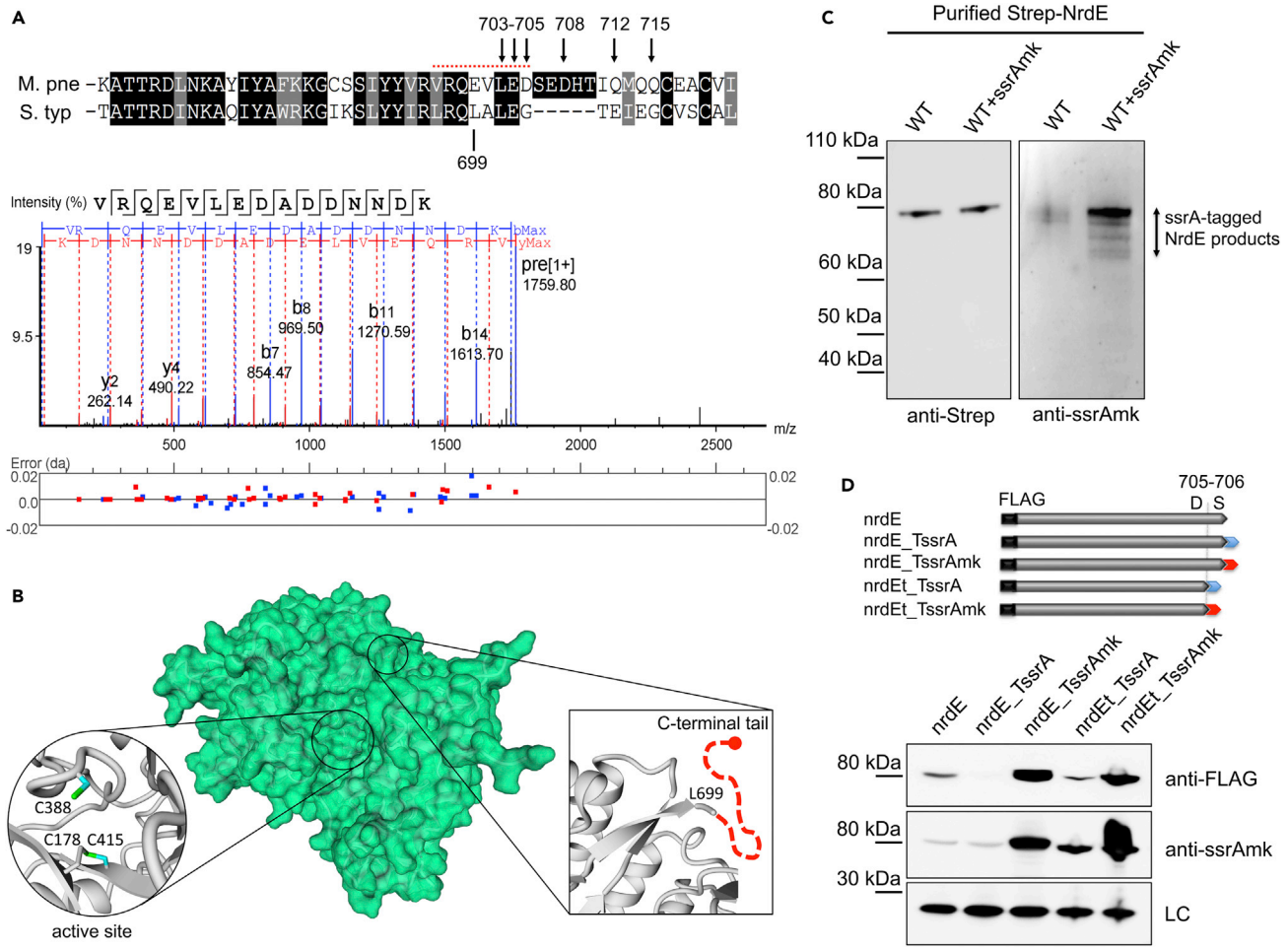

Figure 5. tmRNA tagging in NrdE generates stable C-terminal truncated variants

(A) Sequence alignment between the C-terminal regions of *M. pneumoniae* (M. pne) and *Salmonella typhimurium* (S. typ) NrdE proteins. The amino acid position of the tmRNA tagging sites identified in the *M. pneumoniae* NrdE protein are indicated by arrows. Below, a representative example of a mass spectrum of a NrdE tagged peptide containing both ssrAmk-tag and NrdE sequences. The position of this particular tryptic peptide is highlighted by a red dotted line in the NrdE alignment.

(B) Surface view of the structure of the NrdE protein of *S. typhimurium* (1pem), showing the location of the active-site cleft and the C-terminal mobile tail containing the pair of redox-active cysteines.

(C) N-terminally Strep-tagged NrdE variants were purified from wild-type (WT) and *M. pneumoniae* cells expressing the *ssrAmk* variant. Western blot analysis using anti-Strep and anti-ssrAmk antibodies confirmed tmRNA tagging in NrdE.

(D) Assessment of protein stability of NrdE truncated variants generated by tmRNA tagging. FLAG-tagged derivatives of a representative NrdE truncated variant (same as shown in panel A) containing C-terminal fusions to wild-type or the ssrAmk mutant tag were expressed in wild-type *M. pneumoniae* cells. As controls, similar FLAG-tagged derivatives containing the full NrdE protein sequence were constructed. Stability of the different NrdE derivative versions was assessed by Western blot analysis using anti-FLAG and anti-ssrAmk antibodies. LC, loading control.

with Lon-mediated degradation, both fusion constructs were only detected in the absence of Lon, suggesting the existence of a Lon-degradation signal within the last 25 amino acids of NrdE.

DISCUSSION

Protein quality control mechanisms are critical to maintain proteome homeostasis. These mechanisms act at different levels, preventing either the production of aberrant proteins that can result toxic, or directly refolding or degrading them. Mycoplasmas have undergone a process of reductive evolution, being considered one of the simplest self-replicating organisms. As a result, these bacteria possess a reduced set of genes encoding protein quality control systems, which nevertheless appear to be sufficient to preserve a balanced level of protein homeostasis (Burgos et al., 2020). Mycoplasmas are also considered

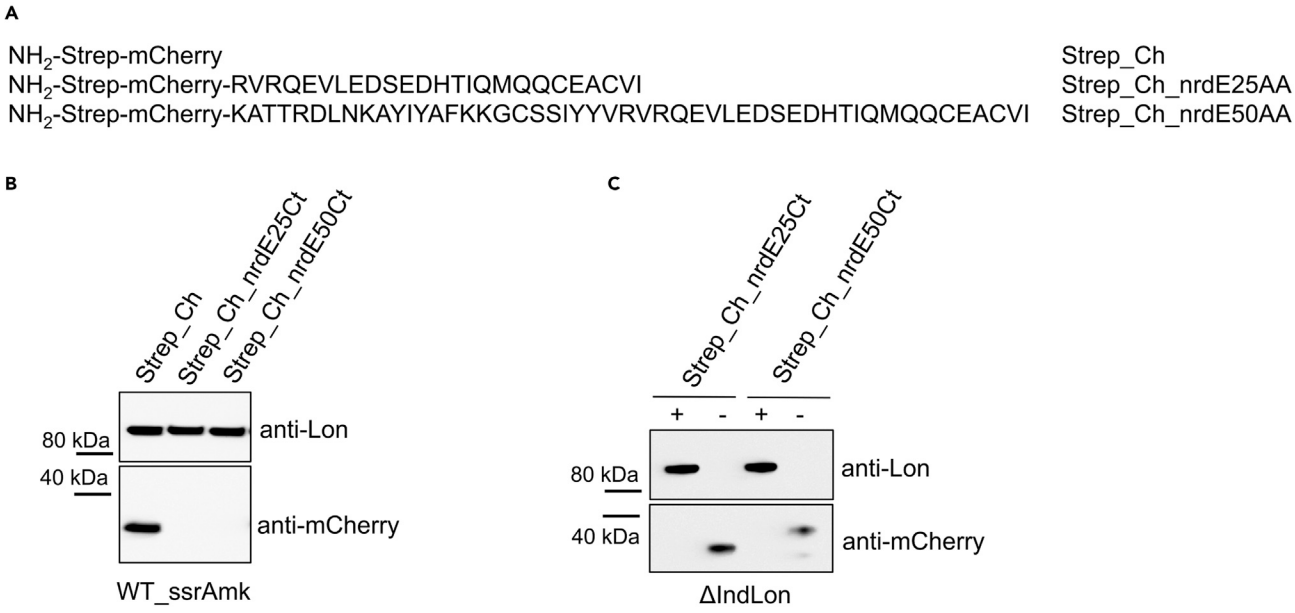

Figure 6. The C-terminal region of NrdE functions as a Lon degron

(A) Schematic representation showing the C-terminal fusions of the mCherry protein with the last 25 and 50 amino acids of NrdE.

(B) Protein stability of mCherry fusions in the WT_ssrAmk strain assessed by Western blot using anti-mCherry antibodies. Lon expression detected by anti-Lon antibodies was used as loading control.

(C) Protein stability of mCherry fusions in the ΔIndLon strain grown under inducing (+) or depleting (−) conditions. Protein expression was assessed by Western blot using anti-mCherry and anti-Lon antibodies.

See also Figure S8.

rapidly evolving bacteria (Woese, 1987). In fact, some species have deficient proofreading systems required to safeguard the fidelity of mRNA translation, producing as a result statistical proteomes (Li et al., 2011; Melnikov et al., 2018). Although these evolutionary strategies can be advantageous in certain conditions, their cost-effectiveness depends on effective systems of dedicated chaperones and proteases capable of maintaining proteome stability. In this regard, with a reduced number of genes encoding chaperone and protease systems, mycoplasmas are interesting cell models to study mechanisms involved in protein quality control.

In the present study we used a combination of genetic and proteomic analysis to characterize the functional activity of the tmRNA system and its potential contribution to translational regulation in *M. pneumoniae*. We provide evidence that the tmRNA system is essential in this model organism due to its ability in releasing stalled ribosomes rather than its role in tagging mistranslated proteins for degradation. These results are consistent with the fact that tmRNA is the only ribosome rescue system present in mycoplasmas and that this bacterium has a small number of ribosomes (Maier et al., 2011). While accumulation of tmRNA-tagged proteins during normal growth conditions does not produce significant toxic effects in *M. pneumoniae*, it is possible that degradation of these products becomes necessary under conditions that favors increased ribosome stalling. Remarkably, we did not see transcriptional activation of the chaperone network of *M. pneumoniae* in the *ssrAmk* mutants, suggesting that basal chaperone expression is enough to cope with possible toxic effects. We found that almost the whole set of chaperones of *M. pneumoniae* was co-purified with tmRNA substrates. Aside from GroEL, we also detected tagged peptides for ClpB and DnaK when relaxing the quality control criteria used for peptide identification. This could explain in part the enrichment of chaperones after the pull down experiments, but it could be also interpreted as that the chaperone network is actively interacting with tmRNA-tagged substrates.

Our study demonstrates that the unusual long tag encoded by the *M. pneumoniae* tmRNA serves as an efficient degradation signal *in vivo*, and that is mainly recognized by the Lon protease. In *E. coli*, both Lon and FtsH have been shown to degrade cytosolic ssrA-tagged proteins (Herman et al., 1998; Choy et al., 2007), although ClpXP seems to be the major protease system involved in this species

(Gottesman et al., 1998). In this case, the action of the SspB protein adaptor is key in delivering ssrA-tagged proteins for ClpXP degradation in an efficient way (Levchenko et al., 2000). With only two ATP-dependent proteases and lacking protease adaptors aiding substrate specificity, we have recently proposed that *M. pneumoniae* has evolved to take advantage of the ability of Lon to recognize accessible hydrophobic regions to regulate protein degradation (Burgos et al., 2020). This implies co-evolution of Lon and their substrates to maximize recognition, especially for those native proteins that are conditionally regulated by proteolysis. The unusual long ssrA-tag of mycoplasmas, enriched with hydrophobic and aromatic residues, illustrates this co-evolution as previously suggested (Gur and Sauer, 2008; Ge and Wali Karzai, 2009).

Quantitative analysis of the major components of the *M. pneumoniae* tmRNA system indicates that there exists one tmRNA system for every 10 ribosomes. This ratio seems to be slightly lower in fast-growing bacteria. This suggests that there may be a selection pressure under high growth rate conditions to decrease the number of improperly terminated RNAs, or that the additional ribosomal content may allow a higher capacity minimizing the toxicity of ribosome stalling. Interestingly, we found that Lon and some chaperone proteins, particularly the GroEL/ES system, are found relatively more abundant in slow-growing bacteria. A model of proteostasis in *E. coli* considering different growth rates predicts that the cell needs higher chaperone levels in two situations: fast growth when protein production is high and aggregation is more likely and very slow growth in order to mitigate the effects of protein degradation (Santra et al., 2017). Our observations suggest that in slow-growing bacteria protein degradation has a major role in maintaining proteome homeostasis, probably as a result of an accumulation of aged proteins derived from a lower protein synthesis rate. A higher capacity of chaperone function seems also beneficial in this situation in order to counteract protein aggregation of aged proteins and increase their potential half-life.

Our study also showed extensive tmRNA activity across the proteome of *M. pneumoniae*. The origin for this activity is unclear, but the existence of premature transcription termination or degradation events generating transcripts lacking stop codons could be possible triggering factors. Close examination of the tagged sites did not reveal rare codon repeats (Roche and Sauer, 1999), or shared sequence motifs that could explain ribosome stalling and subsequent tmRNA tagging. However, we found that hydrophobic and polar uncharged amino acids tend to be more present within the last residues preceding the tagging site. It is possible that these amino acids tend to interact strongly with distinct components of the peptidyl transferase center and the exit tunnel of the ribosome, thereby slowing down the progression of translation. In this regard, known ribosome arrest peptides such as those found in SecM or MifM have in common that interact extensively with the ribosome (Ito and Chiba, 2013). Additionally, three proteins including Def, RpsT, and GroEL were found to be tagged at the very end, suggesting that the efficiency of translation termination in these proteins could be affected as previously observed for other tmRNA-tagged substrates (Roche and Sauer, 2001).

We identified NrdE as one of the major targets of tmRNA activity in *M. pneumoniae*. NrdE is the catalytic subunit of the RNR enzyme that mediates the synthesis of DNA precursors needed for DNA synthesis. In the case of class Ib RNRs, the enzyme comprises two homodimeric subunits named NrdE (α subunit) and NrdF (β subunit), the latter containing the metallocofactor required for the initiation of nucleotide reduction (Torrents, 2014). During the RNR catalysis, there is the formation of a disulfide bond in the active site of NrdE that needs to be reduced to initiate a new cycle of catalysis. Structural studies have shown that the narrow active site cleft of the subunit α does not allow direct reduction by external dithiol-dependent redoxins (Uhlin and Eklund, 1994). Instead, this reduction is performed by a pair of conserved cysteines located at the mobile hydrophobic C-terminal end of NrdE that acts as a shuttle redox system (Sengupta and Holmgren, 2014). Interestingly, we found that NrdE is subject to extensive tmRNA tagging at different sites across the C-terminal region, generating truncated NrdE variants lacking the C-terminal cysteine pair. To our surprise, these truncated variants were stable even when they were fused to the wild-type ssrA degradation tag. One possible hypothesis accounting for this observation is that the ssrA-tag may not be always accessible to the Lon protease. In fact, the ssrA-tag sequence of the truncated variants would substitute the C-terminal mobile tail of NrdE that is thought to enter the active site during each catalytic cycle. This would offer a time-window of protection enabling the NrdE tagged variant to escape from degradation. In fact, our results showed that the C-terminal tail of wild-type NrdE also contains a Lon-degradation signal. Therefore, NrdE may use a similar mechanism to escape from degradation and regulate the half-life of uncomplexed subunits. Additionally, although NrdE truncated variants are expected to

be inactive due to the lack of the C-terminal cysteine pair, they could in principle form stable complexes with normal NrdE and NrdF subunits. This suggests the possibility that NrdE tagged variants could play a role inactivating functional RNR enzymes, similar to the role of Sml1 that precludes the regeneration of the active site of RNR in yeast (Zhang et al., 2007). Intriguingly, class Ib RNR enzymes lack a complete ATP-cone domain that functions as a regulatory allosteric site modulating enzyme activity (Torrents, 2014). Accordingly, class Ib RNR has been generally reported to be insensitive to inhibition by dATP. The sole exception described so far is the NrdE from *B. subtilis* that contains a truncated ATP-cone capable of displaying a class Ia-like activity regulation modulated by dAMP (Parker et al., 2014, Parker et al., 2018). However, sequence conservation analysis of the dAMP binding site predicts only a limited subset of NrdE homologs that may exhibit inhibition by dATP and dAMP (Parker et al., 2018). Therefore, alternative mechanisms regulating the overall activity of RNR may exist.

In summary, we show that a minimal form of cellular life such as *M. pneumoniae*, which contains only about 200 ribosomes per cell, possesses an active system to alleviate ribosome stalling. This system is also efficient in tagging the resulting truncated proteins for degradation, a process mediated by the Lon protease without the apparent aid of protein adaptors. Our results suggest a model in which co-evolution of the sole cytosolic ATP-dependent protease present in *M. pneumoniae*, and their substrates can offer simple mechanisms of regulation without the need of other specialized degradation machineries. In this regard, it has been shown that Lon recognizes sequences relatively rich in hydrophobic residues, enabling Lon to potentially degrade a large substrate repertoire. Intriguingly, cytoplasmic proteins in mycoplasmas have less hydrophobic residues and reduced numbers of long hydrophobic stretches compared to other species (Wong and Houry, 2004). This apparent loss of hydrophobicity may be the result of a selective pressure imposed by Lon surveillance, which seems to play a central role in modulating protein decay in mycoplasmas. Our observations also support the notion that the conformational dynamics of the substrate and its protein-protein interactions can modulate the half-life of the protein. Thus, it is possible that structural characteristics of the substrates have been refined under the same selective pressure. We propose that this evolutionary process possibly contributed to reducing the gene set required for maintaining proteome homeostasis in genome-reduced organisms.

Limitations of the study

Although here we provide evidences of extensive tmRNA tagging at the C-terminal region of NrdE, further studies are warranted to address the underlying mechanism producing stable C-terminal truncated NrdE variants and the potential contribution modulating NrdE activity.

STAR★METHODS

Detailed methods are provided in the online version of this paper and include the following:

- KEY RESOURCES TABLE
- RESOURCE AVAILABILITY
  - Lead contact
  - Materials availability
  - Data and code availability
- EXPERIMENTAL MODEL AND SUBJECT DETAILS
  - Bacterial strains and culture conditions
- METHODS DETAILS
  - Molecular cloning and construction of plasmids
  - Construction of *ssrA* mutants
  - Growth curve analysis
  - RNA sample preparation and RNA-seq analyses
  - Production of anti-ssrAmk antibodies
  - Immunoprecipitation and enrichment of tmRNA substrates
  - Mass spectrometry analyses and identification of tmRNA candidate substrates
  - Immunoblot analysis
  - Expression and purification of strep-tagged proteins
  - Comparative analysis of relative protein abundances in slow and fast-growing bacteria
  - Mass spectrometry analyses of *M. hyopneumoniae* and *M. feriruminatoris*
- QUANTIFICATION AND STATISTICAL ANALYSIS

SUPPLEMENTAL INFORMATION

Supplemental information can be found online at https://doi.org/10.1016/j.isci.2021.102985.

ACKNOWLEDGMENTS

This work has been supported by the European Research Council (ERC) under the European Union's Horizon 2020 research and innovation program under grant agreement 670216 (MYCOCHASSIS), and Conveni La Caixa 2020–2023 (LA CAIXA-EGA, LCF/PR/GN13/10260009). We also acknowledge the support of the Spanish Ministry of Science and Innovation to the EMBL partnership, the Centro de Excelencia Severo Ochoa, and the CERCA Program from the Generalitat de Catalunya. M.W acknowledges the European Union's Horizon 2020 research and innovation program under grant agreement 634942 (MycoSynVac).

We also acknowledge the staff of the CRG Genomics Unit for performing RNA-seq library preparation and sequencing. The proteomics analyses were performed in the CRG/UPF Proteomics Unit which is part of the Proteored, PRB3 and is supported by grant PT17/0019, of the PE I + D + i 2013–2016, funded by ISCIII and ERDF. We also want to thank Ariadna Montero-Blay and Tony Ferrar for sharing MS data and Professor Herrmann for sharing antibodies.

AUTHOR CONTRIBUTIONS

Conceptualization, R.B. and L.S.; methodology, formal analysis, and visualization, R.B. and M.W.; investigation, R.B., and C.G.; writing –original draft, R.B.; writing – review & editing, R.B., M.W., C.G., M.L.-S., and L.S; funding acquisition, L.S; supervision, M.L.-S. and L.S.

DECLARATION OF INTERESTS

The authors declare no competing interests.

Received: May 27, 2021
Revised: July 22, 2021
Accepted: August 11, 2021
Published: September 24, 2021

REFERENCES

Andini, N., and Nash, K.A. (2011). Expression of tmRNA in mycobacteria is increased by antimicrobial agents that target the ribosome. FEMS Microbiol. Lett. *322*, 172–179.

Barends, S., Barend, K., and van Wezel, G.P. (2011). The tmRNA-tagging mechanism and the control of gene expression: a review. Wiley Interdiscip. Rev. RNA *2*, 233–246. https://doi.org/10.1002/wrna.48.

Beer, L.A., Liu, P., Ky, B., Barnhart, K.T., and Speicher, D.W. (2017). Efficient quantitative comparisons of plasma proteomes using label-free analysis with MaxQuant. Methods Mol. Biol. *1619*, 339–352.

Benjamini, Y., and Hochberg, Y. (1995). Controlling the false discovery rate: a practical and powerful approach to multiple testing. J. R. Stat. Soc. Ser. B, 289–300. https://doi.org/10.1111/j.2517-6161.1995.tb02031.x.

Bosdriesz, E., Molenaar, D., Teusink, B., and Bruggeman, F.J. (2015). How fast-growing bacteria robustly tune their ribosome concentration to approximate growth-rate maximization. FEBS J. *282*, 2029–2044.

Bremer, H., and Dennis, P.P. (2008). Modulation of chemical composition and other parameters of the cell at different exponential growth rates. EcoSal Plus *3*. https://doi.org/10.1128/ecosal.5.2.3.

Burgos, R., and Totten, P.A. (2014). Characterization of the operon encoding the Holliday junction helicase RuvAB from Mycoplasma genitalium and its role in mgpB and mgpC gene variation. J. Bacteriol. *196*, 1608–1618.

Burgos, R., Weber, M., Martinez, S., Lluch-Senar, M., and Serrano, L. (2020). Protein quality control and regulated proteolysis in the genome-reduced organism Mycoplasma pneumoniae. Mol. Syst. Biol. *16*, e9530.

Buskirk, A.R., and Green, R. (2017). Ribosome pausing, arrest and rescue in bacteria and eukaryotes. Philos. Trans. R. Soc. Lond. Ser. B Biol. Sci. *372*, 20160183. https://doi.org/10.1098/rstb.2016.0183.

Byun, Y., and Han, K. (2006). PseudoViewer: web application and web service for visualizing RNA pseudoknots and secondary structures. Nucleic Acids Res. *34*, W416–W422.

Chadani, Y., Ono, K., Ozawa, S.-I., Takahashi, Y., Takai, K., Nanamiya, H., Tozawa, Y., Kutsukake, K., and Abo, T. (2010). Ribosome rescue by Escherichia coli ArfA (YhdL) in the absence of trans-translation system. Mol. Microbiol. *78*, 796–808.

Chiva, C., Olivella, R., Borràs, E., Espadas, G., Pastor, O., Solé, A., and Sabidó, E. (2018). QCloud: a cloud-based quality control system for mass spectrometry-based proteomics laboratories. PLoS One *13*, e0189209.

Choy, J.S., Aung, L.L., and Karzai, A.W. (2007). Lon protease degrades transfer-messenger RNA-tagged proteins. J. Bacteriol. *189*, 6564–6571.

Doma, M.K., and Parker, R. (2007). RNA quality control in eukaryotes. Cell *131*, 660–668.

Domingues, S., Moreira, R.N., Andrade, J.M., dos Santos, R.F., Bárria, C., Viegas, S.C., and Arraiano, C.M. (2015). The role of RNase R in trans-translation and ribosomal quality control. Biochimie *114*, 113–118. https://doi.org/10.1016/j.biochi.2014.12.012.

Feaga, H.A., Viollier, P.H., and Keiler, K.C. (2014). Release of nonstop ribosomes is essential. mBio *5*, e01916.

Gallie, D.R. (1991). The cap and poly(A) tail function synergistically to regulate mRNA

translational efficiency. Genes Dev. *5*, 2108–2116. https://doi.org/10.1101/gad.5.11.2108.

Ge, Z., and Wali Karzai, A. (2009). Co-evolution of multipartite interactions between an extended tmRNA tag and a robust Lon protease inMycoplasma. Mol. Microbiol. *74*, 1083–1099. https://doi.org/10.1111/j.1365-2958.2009.06923.x.

Gessulat, S., Schmidt, T., Zolg, D.P., Samaras, P., Schnatbaum, K., Zerweck, J., Knaute, T., Rechenberger, J., Delanghe, B., Huhmer, A., et al. (2019). Prosit: proteome-wide prediction of peptide tandem mass spectra by deep learning. Nat. Methods *16*, 509–518.

Giudice, E., Macé, K., and Gillet, R. (2014). Trans-translation exposed: understanding the structures and functions of tmRNA-SmpB. Front. Microbiol. *5*, 113.

Goralski, T.D.P., Kirimanjeswara, G.S., and Keiler, K.C. (2018). A new mechanism for ribosome rescue can recruit RF1 or RF2 to nonstop ribosomes. mBio *9*. e02436–18. https://doi.org/10.1128/mBio.02436-18.

Gottesman, S., Roche, E., Zhou, Y., and Sauer, R.T. (1998). The ClpXP and ClpAP proteases degrade proteins with carboxy-terminal peptide tails added by the SsrA-tagging system. Genes Dev. *12*, 1338–1347.

Gur, E., and Sauer, R.T. (2008). Evolution of the ssrA degradation tag in Mycoplasma: specificity switch to a different protease. Proc. Natl. Acad. Sci. U S A *105*, 16113–16118.

Hasselbring, B.M., Sheppard, E.S., and Krause, D.C. (2012). P65 truncation impacts P30 dynamics during Mycoplasma pneumoniae gliding. J. Bacteriol. *194*, 3000–3007.

Hayes, C.S., and Sauer, R.T. (2003). Cleavage of the A site mRNA codon during ribosome pausing provides a mechanism for translational quality control. Mol. Cell *12*, 903–911.

Herman, C., Thevenet, D., Bouloc, P., Walker, G.C., and D'Ari, R. (1998). Degradation of carboxy-terminal-tagged cytoplasmic proteins by the Escherichia coli protease HflB (FtsH). Genes Dev. *12*, 1348–1355. https://doi.org/10.1101/gad.12.9.1348.

Huter, P., Müller, C., Arenz, S., Beckert, B., and Wilson, D.N. (2017). Structural basis for ribosome rescue in bacteria. Trends Biochem. Sci. *42*, 669–680.

Ito, K., and Chiba, S. (2013). Arrest peptides: cis-acting modulators of translation. Annu. Rev. Biochem. *82*, 171–202.

Janssen, B.D., and Hayes, C.S. (2012). The tmRNA ribosome-rescue system. Adv. Protein Chem. Struct. Biol. *86*, 151–191.

Jores, J., Fischer, A., Sirand-Pugnet, P., Thomann, A., Liebler-Tenorio, E.M., Schnee, C., Santana-Cruz, I., Heller, M., and Frey, J. (2013). Mycoplasma feriruminatoris sp. nov., a fast growing Mycoplasma species isolated from wild Caprinae. Syst. Appl. Microbiol. *36*, 533–538. https://doi.org/10.1016/j.syapm.2013.07.005.

Keiler, K.C. (2015). Mechanisms of ribosome rescue in bacteria. Nat. Rev. Microbiol. *13*, 285–297.

Komine, Y., Kitabatake, M., Yokogawa, T., Nishikawa, K., and Inokuchi, H. (1994). A tRNA-like structure is present in 10Sa RNA, a small stable RNA from Escherichia coli. Proc. Natl. Acad. Sci. U S A *91*, 9223–9227.

Langmead, B., and Salzberg, S.L. (2012). Fast gapped-read alignment with Bowtie 2. Nat. Methods *9*, 357–359.

Levchenko, I., Seidel, M., Sauer, R.T., and Baker, T.A. (2000). A specificity-enhancing factor for the ClpXP degradation machine. Science *289*, 2354–2356.

Li, L., Boniecki, M.T., Jaffe, J.D., Imai, B.S., Yau, P.M., Luthey-Schulten, Z.A., and Martinis, S.A. (2011). Naturally occurring aminoacyl-tRNA synthetases editing-domain mutations that cause mistranslation in Mycoplasma parasites. Proc. Natl. Acad. Sci. U S A *108*, 9378–9383.

Li, G.-W., Burkhardt, D., Gross, C., and Weissman, J.S. (2014). Quantifying absolute protein synthesis rates reveals principles underlying allocation of cellular resources. Cell *157*, 624–635.

Li, X., Yagi, M., Morita, T., and Aiba, H. (2008). Cleavage of mRNAs and role of tmRNA system under amino acid starvation in Escherichia coli. Mol. Microbiol. *68*, 462–473. https://doi.org/10.1111/j.1365-2958.2008.06167.x.

Lluch-Senar, M., Delgado, J., Chen, W.-H., Lloréns-Rico, V., O'Reilly, F.J., Wodke, J.A., Unal, E.B., Yus, E., Martínez, S., Nichols, R.J., et al. (2015). Defining a minimal cell: essentiality of small ORFs and ncRNAs in a genome-reduced bacterium. Mol. Syst. Biol. *11*, 780.

Maier, T., Schmidt, A., Güell, M., Kühner, S., Gavin, A.-C., Aebersold, R., and Serrano, L. (2011). Quantification of mRNA and protein and integration with protein turnover in a bacterium. Mol. Syst. Biol. *7*, 511.

Mariscal, A.M., Kakizawa, S., Hsu, J.Y., Tanaka, K., González-González, L., Broto, A., Querol, E., Lluch-Senar, M., Piñero-Lambea, C., Sun, L., et al. (2018). Tuning gene activity by inducible and targeted regulation of gene expression in minimal bacterial cells. ACS Synth. Biol. *7*, 1538–1552.

Melnikov, S.V., van den Elzen, A., Stevens, D.L., Thoreen, C.C., and Söll, D. (2018). Loss of protein synthesis quality control in host-restricted organisms. Proc. Natl. Acad. Sci. U S A *115*, E11505–E11512.

Miravet-Verde, S., Ferrar, T., Espadas-García, G., Mazzolini, R., Gharrab, A., Sabido, E., Serrano, L., and Lluch-Senar, M. (2019). Unraveling the hidden universe of small proteins in bacterial genomes. Mol. Syst. Biol. *15*, e8290.

Moore, S.D., and Sauer, R.T. (2005). Ribosome rescue: tmRNA tagging activity and capacity in Escherichia coli. Mol. Microbiol. *58*, 456–466.

Müller, C., Crowe-McAuliffe, C., and Wilson, D.N. (2021). Ribosome rescue pathways in bacteria. Front. Microbiol. *12*, 652980.

Muth, T., and Renard, B.Y. (2018). Evaluating de novo sequencing in proteomics: already an accurate alternative to database-driven peptide identification? Brief. Bioinformatics *19*, 954–970.

Nakatogawa, H., Murakami, A., and Ito, K. (2004). Control of SecA and SecM translation by protein secretion. Curr. Opin. Microbiol. *7*, 145–150.

Nam, D., Choi, E., Shin, D., and Lee, E.-J. (2016). tRNAPro-mediated downregulation of elongation factor P is required for mgtCBR expression during Salmonella infection. Mol. Microbiol. *102*, 221–232. https://doi.org/10.1111/mmi.13454.

Parker, M.J., Maggiolo, A.O., Thomas, W.C., Kim, A., Meisburger, S.P., Ando, N., Boal, A.K., and Stubbe, J. (2018). An endogenous dAMP ligand in Bacillus subtilis class Ib RNR promotes assembly of a noncanonical dimer for regulation by dATP. Proc. Natl. Acad. Sci. *115*, E4594–E4603. https://doi.org/10.1073/pnas.1800356115.

Parker, M.J., Zhu, X., and Stubbe, J. (2014). Bacillus subtilis class Ib ribonucleotide reductase: high activity and dynamic subunit interactions. Biochemistry *53*, 766–776.

Perez-Riverol, Y., Csordas, A., Bai, J., Bernal-Llinares, M., Hewapathirana, S., Kundu, D.J., Inuganti, A., Griss, J., Mayer, G., Eisenacher, M., et al. (2019). The PRIDE database and related tools and resources in 2019: improving support for quantification data. Nucleic Acids Res. *47*, D442–D450.

Perkins, D.N., Pappin, D.J., Creasy, D.M., and Cottrell, J.S. (1999). Probability-based protein identification by searching sequence databases using mass spectrometry data. Electrophoresis *20*, 3551–3567.

Personne, Y., and Parish, T. (2014). Mycobacterium tuberculosis possesses an unusual tmRNA rescue system. Tuberculosis *94*, 34–42.

Pich, O.Q., Burgos, R., Planell, R., Querol, E., and Piñol, J. (2006). Comparative analysis of antibiotic resistance gene markers in Mycoplasma genitalium: application to studies of the minimal gene complement. Microbiology *152*, 519–527.

Piñero-Lambea, C., Garcia-Ramallo, E., Martinez, S., Delgado, J., Serrano, L., and Lluch-Senar, M. (2020). Genome editing based on oligo recombineering and Cas9-mediated Counterselection. ACS Synth. Biol. *9*, 1693–1704.

Reynolds, N.M., Lazazzera, B.A., and Ibba, M. (2010). Cellular mechanisms that control mistranslation. Nat. Rev. Microbiol. *8*, 849–856.

Robinson, M.D., McCarthy, D.J., and Smyth, G.K. (2010). edgeR: a Bioconductor package for differential expression analysis of digital gene expression data. Bioinformatics *26*, 139–140.

Robinson, M.D., and Oshlack, A. (2010). A scaling normalization method for differential expression analysis of RNA-seq data. Genome Biol. *11*, R25.

Robinson, M.D., and Smyth, G.K. (2007). Moderated statistical tests for assessing differences in tag abundance. Bioinformatics *23*, 2881–2887.

Robinson, M.D., and Smyth, G.K. (2008). Small-sample estimation of negative binomial dispersion, with applications to SAGE data. Biostatistics *9*, 321–332.

Roche, E.D., and Sauer, R.T. (1999). SsrA-mediated peptide tagging caused by rare codons and tRNA scarcity. EMBO J. *18*, 4579–4589.

Roche, E.D., and Sauer, R.T. (2001). Identification of endogenous SsrA-tagged proteins reveals tagging at positions corresponding to stop codons. J. Biol. Chem. *276*, 28509–28515.

Santra, M., Farrell, D.W., and Dill, K.A. (2017). Bacterial proteostasis balances energy and chaperone utilization efficiently. Proc. Natl. Acad. Sci. U S A *114*, E2654–E2661.

Schmidl, S.R., Hames, C., and Stülke, J. (2007). Expression of mycoplasma proteins carrying an affinity tag in M. Pneumoniae allows rapid purification and circumvents problems related to the aberrant genetic code. Appl. Environ. Microbiol. *73*, 7799–7801. https://doi.org/10.1128/aem.01861-07.

Schmidt, T., Samaras, P., Dorfer, V., Panse, C., Kockmann, T., Bichmann, L., van Puyvelde, B., Perez-Riverol, Y., Deutsch, E.W., Kuster, B., et al. (2021). Universal spectrum explorer: a standalone (Web-)Application for cross-resource spectrum comparison. J. Proteome Res. *20*, 3388–3394.

Sengupta, R., and Holmgren, A. (2014). Thioredoxin and glutaredoxin-mediated redox regulation of ribonucleotide reductase. World J. Biol. Chem. *5*, 68–74.

Seybert, A., Herrmann, R., and Frangakis, A.S. (2006). Structural analysis of Mycoplasma pneumoniae by cryo-electron tomography. J. Struct. Biol. *156*, 342–354.

Shimokawa-Chiba, N., Müller, C., Fujiwara, K., Beckert, B., Ito, K., Wilson, D.N., and Chiba, S. (2019). Release factor-dependent ribosome rescue by BrfA in the Gram-positive bacterium Bacillus subtilis. Nat. Commun. *10*, 5397.

Sperschneider, J., and Datta, A. (2010). DotKnot: pseudoknot prediction using the probability dot plot under a refined energy model. Nucleic Acids Res. *38*, e103. https://doi.org/10.1093/nar/gkq021.

Sturm, M., Schroeder, C., and Bauer, P. (2016). SeqPurge: highly-sensitive adapter trimming for paired-end NGS data. BMC Bioinformatics *17*, 208.

Torrents, E. (2014). Ribonucleotide reductases: essential enzymes for bacterial life. Front. Cell. Infect. Microbiol. *4*, 52.

Tully, J.G., Rose, D.L., Whitcomb, R.F., and Wenzel, R.P. (1979). Enhanced isolation of Mycoplasma pneumoniae from throat washings with a newly-modified culture medium. J. Infect. Dis. *139*, 478–482.

Uhlin, U., and Eklund, H. (1994). Structure of ribonucleotide reductase protein R1. Nature *370*, 533–539.

Wang, M., Herrmann, C.J., Simonovic, M., Szklarczyk, D., and von Mering, C. (2015). Version 4.0 of PaxDb: protein abundance data, integrated across model organisms, tissues, and cell-lines. Proteomics *15*, 3163–3168.

Weber, M., Burgos, R., Yus, E., Yang, J.-S., Lluch-Senar, M., and Serrano, L. (2020). Impact of C-terminal amino acid composition on protein expression in bacteria. Mol. Syst. Biol. *16*, e9208.

Wickner, S., Maurizi, M.R., and Gottesman, S. (1999). Posttranslational quality control: folding, refolding, and degrading proteins. Science *286*, 1888–1893.

Woese, C.R. (1987). Bacterial evolution. Microbiol. Rev. *51*, 221–271. https://doi.org/10.1128/mmbr.51.2.221-271.1987.

Wong, P., and Houry, W.A. (2004). Chaperone networks in bacteria: analysis of protein homeostasis in minimal cells. J. Struct. Biol. *146*, 79–89.

Yamamoto, Y., Sunohara, T., Jojima, K., Inada, T., and Aiba, H. (2003). SsrA-mediated trans-translation plays a role in mRNA quality control by facilitating degradation of truncated mRNAs. RNA *9*, 408–418. https://doi.org/10.1261/rna.2174803.

Yus, E., Lloréns-Rico, V., Martínez, S., Gallo, C., Eilers, H., Blötz, C., Stülke, J., Lluch-Senar, M., and Serrano, L. (2019). Determination of the gene regulatory network of a genome-reduced bacterium highlights alternative regulation independent of transcription factors. Cell Syst. *9*, 143–158.e13.

Yus, E., Maier, T., Michalodimitrakis, K., van Noort, V., Yamada, T., Chen, W.-H., Wodke, J.A.H., Güell, M., Martínez, S., Bourgeois, R., et al. (2009). Impact of genome reduction on bacterial metabolism and its regulation. Science *326*, 1263–1268.

Zhang, Z., Yang, K., Chen, C.-C., Feser, J., and Huang, M. (2007). Role of the C terminus of the ribonucleotide reductase large subunit in enzyme regeneration and its inhibition by Sml1. Proc. Natl. Acad. Sci. *104*, 2217–2222. https://doi.org/10.1073/pnas.0611095104.

STAR★METHODS

KEY RESOURCES TABLE

REAGENT or RESOURCE	SOURCE	IDENTIFIER
Antibodies		
Rabbit polyclonal anti-CAT	Abcam	Cat# ab50151; RRID: AB_869140
Mouse monoclonal anti-FLAG M2	Sigma	Cat# F1804; RRID: AB_262044
Strep-Tactin conjugated to HRP	IBA, lifesciences	Cat#2-1502-001
DsRed polyclonal antibody	Takara	Cat# 632496; RRID:AB_10013483
Rabbit polyclonal anti-ssrAmk	This paper	N/A
Rabbit polyclonal anti-Lon	Richard Herrmann lab	N/A
Rabbit polyclonal anti-FtsH	Richard Herrmann lab	N/A
Sheep polyclonal HRP-conjugated anti-mouse IgG	Sigma	Cat# A6782; RRID:AB_258315
Goat polyclonal HRP-conjugated anti-rabbit IgG	Sigma	Cat# A0545; RRID:AB_257896
Bacterial and virus strains		
Mycoplasma pneumoniae M129	Richard Herrmann lab	N/A
Mycoplasma hyopneumoniae 232	Chris Minion lab	N/A
Mycoplasma feriruminatoris G5847	Jores et al., 2013	N/A
Other mycoplasma strains	This paper	See Table S3
Escherichia coli TOP10	Invitrogen	Cat#C404003
Escherichia coli DH5α	New England Biolabs	Cat#C2987H
Chemicals, peptides, and recombinant proteins		
X-Gal solution	Thermo Scientific	Cat#R0941
Puromycin	Gibco	Cat#A1113803
Chlorampehnicol	Sigma	Cat#C0378
Tetracycline	Sigma	Cat#T7660
Gentamycin	Sigma	Cat#G1397
Phusion High-Fidelity DNA Polymerase	Thermo Scientific	Cat#F530S
XhoI	New England Biolabs	Cat#R0146S
EcoRV	New England Biolabs	Cat#R0195S
PstI	New England Biolabs	Cat#R3140S
cOmplete™, EDTA-free Protease Inhibitor Cocktail	Roche	Cat#4693132001
Dynabeads™ MyOne Streptavidin C1	Invitrogen	Cat#65001
Protein G Dynabeads	Invitrogen	Cat#10004D
Tween 20	Sigma	Cat#P7949
RIPA buffer	Sigma	Cat#R0278
Endopeptidase LysC	Wako Pure Chemical	Cat#121-05063
Trypsin	Promega	Cat#V5111
Digested bovine serum albumin	New England Biolabs	Cat#P8108S
Triton X-100	Sigma	Cat#X100
StrepTactin Sepharose High Performance	GE Healthcare	Cat#28-9355-99
d-Desthiobiotin	Sigma	Cat#D1411
Critical commercial assays		
QuikChange Site-Directed Mutagenesis Kit	Agilent Technologies	Cat#200518
BCA Protein assay Kit	Pierce	Cat#23225

(*Continued on next page*)

Continued

REAGENT or RESOURCE	SOURCE	IDENTIFIER
miRNeasy Mini Kit	Qiagen	Cat#217004
TruSeq Stranded mRNA Sample Prep Kit v2	Illumina	Cat#RS-122-2101
NuPAGE 4-12% Bis-Tris pre-cast polyacrylamide gels	Invitrogen	Cat#WG1402BX10
Supersignal West Femto Chemiluminescent Substrate	Thermo Scientific	Cat#34096
Supersignal West Pico Chemiluminescent Substrate	Thermo Scientific	Cat#34080
Deposited data		
RNA sequencing data	This paper	ArrayExpress: E-MTAB-10111
tmRNA tagging proteomics data	This paper	PRIDE: PXD023973
M. hyopneumoniae and *M. feriruminatoris* proteomics data	This paper	PRIDE: PXD025422
Proteomics data of other mycoplasma species	Miravet-Verde et al., 2019	PRIDE: PXD008243
Proteomics data *E. coli*	Li et al., 2014	EcoCyc: https://ecocyc.org
Other proteomics data	(Wang et al., 2015)	PaxDB: https://pax-db.org/
M. pneumoniae M129 reference genome	NCBI	NC_000912.1
Oligonucleotides		
Primers	This paper	See Table S4
Recombinant DNA		
pBSKII+	Stratagene	Cat#212205
pMTnCat	Burgos and Totten (2014)	N/A
pMTnCat(lox)	Burgos et al. (2020)	N/A
pMTnTetM438	Pich et al. (2006)	N/A
pMTnGm	Pich et al. (2006)	N/A
Other plasmids	This paper	See Table S5
Software and algorithms		
Proteome Discoverer (v2.0 and v2.3)	Thermo Fisher Scientific	N/A
Mascot search engine (v2.5)	Matrix Science	N/A
Xcalibur software (v2.2)	Thermo Fisher Scientific	N/A
PEAKS Studio (v7.0)	Bioinformatics Solutions Inc	N/A
edgeR (v3.26.8)	Robinson et al. (2010)	N/A
SeqPurge tool (v0.1-478-g3c8651b)	Sturm et al. (2016)	N/A
bowtie2 (v2.3.5)	Langmead and Salzberg (2012)	N/A
DotKnot (v1.3.2)	Sperschneider and Datta (2010)	https://dotknot.csse.uwa.edu.au
Pseudoviewer	Byun and Han (2006)	http://pseudoviewer.inha.ac.kr
PROSIT (v1.1.2)	Gessulat et al., 2019	https://github.com/kusterlab/prosit
Universal Spectrum Explorer (USE)	Schmidt et al., 2021	https://www.proteomicsdb.org/use
Other		
Gene Pulser XCell™ electroporation system	Bio-Rad	N/A
Infinite M200 plate reader	Tecan	N/A
HiSeq 2500 sequencing platform	Illumina	N/A
BioAnalyzer	Agilent	N/A
iBlotTM dry blotting system	Invitrogen	N/A
LAS-3000 Imaging System	Fujifilm	N/A
Bioruptor sonication system	Diagenode	N/A
LTQ-Orbitrap Fusion Lumos mass spectrometer	Thermo Fisher	N/A
LTQ-Orbitrap Velos Pro mass spectrometer	Thermo Fisher	N/A

RESOURCE AVAILABILITY

Lead contact

Further information and requests for resources and reagents should be directed to and will be fulfilled by the lead contact, Luis Serrano (luis.serrano@crg.eu).

Materials availability

Plasmids, strains and antibodies generated in this study are available from the lead contact upon request.

Data and code availability

- The RNA sequencing data have been deposited in ArrayExpress repository with the dataset identifier ArrayExpress: E-MTAB-10111. The mass spectrometry proteomics data have been deposited to the ProteomeXchange Consortium via the PRIDE (Perez-Riverol et al., 2019) partner repository with the dataset identifiers PRIDE: PXD023973 (tmRNA tagging proteomics) and PRIDE: PXD025422 (*M. hyopneumoniae* and *M. feriruminatoris* proteomics). These accession numbers are also listed in the key resources table.
- This paper does not report original code.
- Any additional information required to reanalyze the data reported in this paper is available from the lead contact upon request.

EXPERIMENTAL MODEL AND SUBJECT DETAILS

Bacterial strains and culture conditions

Wild-type *M. pneumoniae* strain M129 and its derivatives (Table S3) were grown in modified Hayflick medium (Yus et al., 2009) at 37°C under 5% CO_2 in tissue culture flasks. *M. hyopneumoniae* 232 and *M. feriruminatoris* G5847 strains were grown in suspension (180 rpm at 37°C) in Hayflick medium without glucose and supplemented with sodium pyruvate 0.5% or SP-4 medium (Tully et al., 1979), respectively. Hayflick medium was supplemented with 0.8% agar when solid medium was required, puromycin (3 μg/ml), chloramphenicol (20 μg/ml), tetracycline (2 μg/ml) or gentamicin (100 μg/ml) was used for selection of transformants as needed. For vector cloning, we used *E. coli* strains TOP10 (Invitrogen) and Dh5α (New England Biolabs) grown at 37°C in LB broth or LB agar plates containing ampicillin (100 μg/ml) and X-Gal (40 μg/ml).

METHODS DETAILS

Molecular cloning and construction of plasmids

Primers and plasmids generated in this study are summarized in Tables S4 and S5, respectively. *M. pneumoniae* strains listed in Table S3 were obtained by transforming the corresponding plasmids using electroporation (Weber et al., 2020). Briefly, approximately 10^8 cells and 2 μg of DNA were incubated for 15 min in ice-cold electroporation buffer (8 mM HEPES·Na pH 7.2, 272 mM sucrose) in a 1-mm gapped electroporation cuvette (Bio-Rad). Then, cells were electroporated using the Gene Pulser XCell™ electroporation system (Bio-Rad) with the pulse controller set at 1.25 kV, 25 μF, and 100 Ω. After a recovering period of 15 min on ice, cells were resuspended in 900 μl of Hayflick medium and incubated for 2 h at 37°C. Finally, the pool of transformants were selected in liquid or solid medium cultures containing the corresponding antibiotic.

Minitransposons vectors carrying the *cat* reporters fused to the ssrA-tag variants were constructed as follows. First, we amplified both the *cat* gene from pMTnCat plasmid (Burgos and Totten, 2014) using the pair of primers (catTssrA_F / catTssrA_R); and a genomic fragment encompassing the ssrA-tag using the primers catTssrA_F2 and catTssrA_R2. These two fragments were joined by overlapping PCR using primers catTssrA_F and catTssrA_R2, which contain *Xho*I and *Eco*RV restriction sites at their 5′ ends. The PCR product was then cloned into a *Xho*I/*Eco*RV-digested pMTn*TetM438* vector (Pich et al., 2006) generating pMTnTc_cat_TssrA. Since the ΔIndFtsH recipient strain carries a *tetM* resistance gene, a *Xho*I/*Eco*RV-digested pMTnGm vector was used instead to clone the cat_TssrA fusion. A similar strategy was used to construct pMTnTc_catT_ssrAk. In this case, the *cat* gene and the ssrA-tag were amplified using the pair of primers (catTssrA_F / catTssrAk_R) and (catTssrAk_F2 / catTssrA_R2), respectively. Aspartic mutations in the ssrA-tag of plasmids pMTnTc_cat_TssrA and pMTnTc_cat_TssrAk were obtained by QuickChange

PCR mutagenesis using the primer pair (ssrAtagM_F / ssrAtagM_R) generating pMTnTc_cat_TssrAm and pMTnTc_cat_TssrAmk plasmids.

Minitransposons vectors expressing different *ssrA* gene variants were constructed as follows. The wild-type *ssrA* gene sequence including the 189 bp located upstream was amplified using the primer pair (ssrA_F / ssrA_R), which contain *Xho*I and *Eco*RV restriction sites at their 5′ ends. The PCR product was then cloned into a *Xho*I/*Eco*RV-digested pMTnCat (Burgos and Totten, 2014) generating pMTnCat_ssrA. The mutant variant pMTnCat_ssrAmk was created by two consecutive QuickChange PCR mutagenesis rounds using the primer pairs (ssrAk_F / ssrAk_R) and (ssrAtagM_F / ssrAtagM_R). The pMTnCat_p438_ssrAmk vector, which carries the *ssrAmk* mutant variant expressed from the P438 promoter (Pich et al., 2006), was obtained by amplifying *ssrAmk* with primers ssrAp438_F and ssrA_R, and subsequent cloning into a *Xho*I/*Eco*RV-digested pMTnCat vector. Similarly, the *ssrAmk* gene variant with its 5′UTR was also cloned into a *Xho*I/*Eco*RV-digested pMTn*TetM438* vector (Pich et al., 2006) creating pMTnTc_ssrAmk.

To delete the *ssrA* endogenous gene we constructed the suicide plasmid pΔssrA. To do this, a fragment spanning the 5′ flanking sequence of *ssrA* was amplified using primers LA_ssrA_F and LA_ssrA_R. A second fragment containing the *cat* resistance gene flanked by lox sites was amplified with the primer pair (ssrA_lox_cat_F / ssrA_lox_cat_R) and using as a template pMTnCat(lox) (Burgos et al., 2020). A third fragment containing the 3′ flanking sequence of *ssrA* was amplified using primers RA_ssrA_F and RA_ssrA_R. The three PCR products were joined by overlapping PCR using primers ΔssrA_F and ΔssrA_R, which contain *Xho*I and *Pst*I restriction sites at their 5′ ends. Finally, the PCR product was cloned into a *Xho*I/*Pst*I-digested pBSKII+ (Stratagene).

A minitransposon vector aimed to express N-terminal Strep-tagged NrdE proteins was constructed in a two-step PCR strategy, in which the forward primers include the strep-tag and P438 promoter sequences (Pich et al., 2006). Briefly, the NrdE coding sequence was first amplified with primers Strep_ndrE_F and nrdE_R. The resulting PCR product was then used as a template in a second PCR reaction with primers P438_Strep_F and nrdE_R, which contain *Xho*I and *Eco*RV restriction sites at their 5′ ends. The PCR product was finally cloned into a *Xho*I/*Eco*RV-digested pMTn*TetM438* vector (Pich et al., 2006) creating pMTnTc_Strep_nrdE.

Minitransposons vectors expressing N-terminal FLAG-tagged NrdE derivatives were constructed as follows. For pMTnCat_FLAG_nrdE, we used a two step PCR strategy in which the forward primers include the FLAG-tag and P438 promoter sequences (Pich et al., 2006). For this, we used the pair of primers (FLAG_nrdE _F / p_nrdE_R) and (p_P438FLAG _F / p_nrdE_R). The final PCR product was cloned by Gibson assembly into an *Eco*RV-digested pMTnCat vector (Burgos and Totten, 2014). Constructs pMTnCat_FLAG_nrdE_TssrA, pMTnCat_FLAG_nrdE_TssrAmk, pMTnCat_FLAG_nrdEt_TssrA and pMTnCat_FLAG_nrdEt_TssrAmk were engineer to carry NrdE variants fused to the wild-type or the ssrAmk mutant tag. To obtain these vectors, we generated two PCR fragments containing *nrdE* or ssrA-tag sequences that were assembled together by Gibson cloning with an *Eco*RV-digested pMTnCat vector (Burgos and Totten, 2014). The first fragment was amplified from pMTnCat_FLAG_nrdE using the primer pairs (p_P438FLAG _F / nrdE_TssrA_R), (p_P438FLAG _F /nrdE_TssrAmk_R), (p_P438FLAG _F / nrdEt_TssrA_R) or (p_P438FLAG _F / nrdEt_TssrAmk_R), respectively. The second fragment was obtained by using the primer pairs (nrdE_TssrA_F / p_TssrA _R), (nrdE_TssrAmk_F / p_TssrAmk _R), (nrdEt_TssrA_F / p_TssrA _R) or (nrdEt_TssrAmk_F / p_TssrAmk _R), respectively.

Minitransposons vectors expressing mCherry variants were constructed as follows. The mCherry coding sequence was modified to include an in-frame fusion of a 29 amino acid peptide of mp200 ORF. The N-terminal fusion to this peptide was previously shown to improve protein stability (Mariscal et al., 2018). To obtain the pMTnTc_Strep_Cherry control vector, we used a two step PCR strategy in which the forward primers include the strep-tag and P438 promoter sequences (Pich et al., 2006). For this, we used the pair of primers (P438_Strep_Ch_F / p_Ch_R) and (p_P438 _F / p_Ch_R). The final PCR product was cloned by Gibson assembly into an *Eco*RV-digested pMTn*TetM438* vector (Pich et al., 2006). For pMTnTc_Strep_Cherry_nrdE25Ct and pMTnTc_Strep_Cherry_nrdE50Ct constructs containing C-terminal fusions with the last residues of NrdE, we obtained two PCR fragments. A common first fragment containing mCherry sequences was amplified from pMTnTc_Strep_Cherry using p_P438 _F and Ch_noTAA_R primers. A second fragment containing the last 25 or 50 residues of NrdE was obtained using the primer pairs

(Ch_25CtnrdE_F / p_nrdE_R) or (Ch_50CtnrdE_F / p_nrdE_R), respectively. The two PCR fragments were finally assembled together by Gibson cloning into an *Eco*RV-digested pMTn*TetM438* vector (Pich et al., 2006).

Construction of *ssrA* mutants

A *M. pneumoniae* mutant expressing a *ssrA* gene variant encoding a tag resistant to proteolysis (*ssrAmk*) was constructed by transforming the pMTnTc_ssrAmk minitransposon into M129_GP35, a wild-type strain expressing the *gp35* gene (Piñero-Lambea et al., 2020). Transformants were selected in Hayflick agar plates containing 2μg/ml tetracycline obtaining the WT+ssrAmk strain. The endogenous *ssrA* gene from this strain was then deleted by GP35 recombination to obtain the ΔssrA+ssrAmk strain. To perform this deletion we used the plasmid pΔssrA and the pair of primers (Pro_ssrA_F / Bio_ssrA_R) to amplify the dsDNA template that was used to generate the ssDNA recombineering substrate. The primers were designed to contain biotin or phosphorothioate modifications attached to the 5' ends in order to allow ssDNA purification and protection of the ssDNA substrate. The pΔssrA includes a *cat* selectable marker enclosed by *ssrA* flanking regions, allowing complete deletion of *ssrA* and replacement by the *cat* gene. The ssDNA substrate was obtained by Biotin-Streptavidin affinity purification (Burgos et al., 2020) using MyOne^{TM} Streptavidin C1 dynabeads (Invitrogen). To delete the endogenous *ssrA* gene, the WT+ssrAmk strain was electroporated with 3 μg of recombineering substrate and cultured in 5ml cultures during 24h to allow GP35 mediated recombination. Transformants were selected in Hayflick agar plates containing 20μg/ml chloramphenicol, and allelic exchange was verified by PCR analysis using primers LA_ssrA_F and RA_ssrA_R (Figure S7 and Table S4). The specific insertion site of the transposon expressing the *gp35* and *ssrAmk* genes were located in coordinates 499724 and 365099, respectively.

RNA folding and pseudoknot structure of the *M. pneumoniae ssrAmk* gene variant was predicted by running the DotKnot software tool (Sperschneider and Datta, 2010) and visualized through the Pseudoviewer application (Byun and Han, 2006).

Growth curve analysis

Growth curve analyses were performed by measuring protein biomass. Briefly, duplicate 5 ml cultures for each time point were washed with PBSx1 once and cells scraped off from the flasks in 1ml of PBSx1. Then, the cell suspension was harvested by centrifugation (13,100 x g, 10min), and the pellet resuspended in lysis buffer containing 1% SDS and disrupted by sonication using a Bioruptor sonication system (Diagenode) with an On/Off interval time of 30/30 sec at high frequency for 10 min. Finally, duplicate protein measurements were performed using the Pierce ^{TM} BCA Protein Assay Kit.

RNA sample preparation and RNA-seq analyses

RNA was isolated using the miRNeasy kit (Qiagen), including the in-column DNase I treatment, and the quality of RNA assessed using a BioAnalyzer (Agilent). The RNA-seq libraries were prepared at the CRG Genomics Unit using the TruSeq Stranded mRNA Sample Prep Kit v2 following the manufacturer's protocol with few modifications. The poly(A) selection step was omitted and 100 ng of total RNA was used for fragmentation. The library insert sizes were reduced compared to the standard protocol by increasing the amount of AMPure XP beads as follows. After adaptor ligation, 50 μl of beads were used instead of 42 μl. Then, 55 μl AMPure XP beads were used instead of 50 μl for both the second round of bead purification, and the purification of the PCR reaction after library amplification. Sequencing was performed using a HiSeq 2500 (Illumina) with HiSeq v4 chemistry and 2x50 bp paired-end reads.

Processing of sequencing reads was performed as follows. Adapter sequences were trimmed by using the SeqPurge tool (Sturm et al., 2016) keeping trimmed reads with a minimum length of 12. Alignment of reads was performed using bowtie2 tools (Langmead and Salzberg, 2012) with predefined parameters values (Burgos et al., 2020) and using the wild-type reference genome of *M. pneumoniae* M129 (NCBI accession NC_000912.1).

Production of anti-ssrAmk antibodies

Polyclonal antibodies against the ssrAmk-tag were commercially produced by immunizing rabbits with the synthetic peptide DDNNDKVLVDPMLIANQQASIDDDFA and KLH conjugates. Specific IgG antibodies

were recovered from the crude serum by affinity purification. Peptide synthesis, antibody production and affinity purification were performed by Eurogentec (Belgium).

Immunoprecipitation and enrichment of tmRNA substrates

Endogenous protein tagging by tmRNA was examined by immunoprecipitation (IP) enrichment followed by LC-MS/MS analysis. For this, mutant cells expressing the *ssrAmk* gene variant (mutant sample) or wild-type *ssrA* gene (control sample) were grown in duplicate 20 ml cultures. In a first IP enrichment experiment, cells were washed twice with cold PBSx1 and lysed directly into the flask by scraping off the cells in a PBSx1 buffer containing 0.1% SDS plus protease inhibitor cocktail (Roche). Cell extracts were passed several times through a syringe with a 25-gauge needle and incubated at 4°C on a rotating platform for 30 min before being subjected to centrifugation at 18,000 x g for 10 min. Supernatants were then incubated overnight with purified anti-ssrAmk antibodies at 4°C on a rotating platform in four independent binding reactions per sample, each containing 250 μg of protein and 3 μg of antibody. Antibody-protein complexes were captured by incubating the supernatants with Protein G Dynabeads (Invitrogen), which were previously washed twice with PBSx1 containing 0.05% Tween 20. After 4h of incubation with rotation at 4°C, Dynabeads complexes were washed thrice with PBSx1 containing 0.05% Tween 20 and transferred to a clean microtube. After removing the supernatant, Dynabeads complexes were resuspended in a buffer containing (50mM Tris-HCl, pH 7.4; 1% SDS), and incubated at 65°C during 10 min. Finally, supernatants were recovered and pooled for mass spectrometry analysis.

A second IP enrichment experiment was performed using more stringent conditions. Briefly, cells were lysed with RIPA buffer from Sigma (150 mM NaCl, 1.0% IGEPAL® CA-630, 0.5% sodium deoxycholate, 0.1% SDS, 50 mM Tris, pH 8.0) followed by mild sonication using a Bioruptor sonication system (Diagenode) with an On/Off interval time of 30/30 sec at medium frequency for 90 seconds. Cell extracts were then centrifuged at 18,000 x g for 10 min, and subjected to a pre-clearing step (2h in rotation at 4°C) employing Protein G Dynabeads (Invitrogen). Binding reactions of supernatants with anti-ssrAmk antibodies and Protein G Dynabeads were performed as described above, except that Dynabeads complexes were washed five times with PBSx1 containing 0.1% Tween 20. For this experiment, two independent mutant samples were processed.

Mass spectrometry analyses and identification of tmRNA candidate substrates

Sample digestion. Samples were reduced with dithiothreitol (100 mM, 37°C, 60 min) and alkylated in the dark with iodoacetamide (5 μmol, 25°C, 20 min). The resulting protein extract was wash with 2M urea with 100 mM Tris-HCl and then with 50 mM ammonium bicarbonate for digestion with endoproteinase LysC (1:10 w:w, 37°C, o/n, Wako Pure Chemical) and then for trypsin digestion (1:10 w:w, 37°C, 8h, Promega). After digestion, peptide mix was acidified with formic acid and desalted with a MicroSpin C18 column (The Nest Group, Inc) prior to LC-MS/MS analysis.

Mass spectrometry analysis. Samples were analyzed using a LTQ-Orbitrap Fusion Lumos mass spectrometer (Thermo Fisher Scientific, San Jose, CA, USA) coupled to an EASY-nLC 1000 (Thermo Fisher Scientific (Proxeon), Odense, Denmark). Peptides were loaded directly onto the analytical column and were separated by reverse-phase chromatography using a 50-cm column with an inner diameter of 75 μm, packed with 2 μm C18 particles spectrometer (Thermo Scientific, San Jose, CA, USA). Chromatographic gradients were performed as follows. First at 95% buffer A and 5% buffer B with a flow rate of 300 nl/min and then gradually increased to 35% buffer B and 65% A in 60 min. The column was washed for 10 min with 10% buffer A and 90% buffer B after each analysis. Buffer A: 0.1% formic acid in water. Buffer B: 0.1% formic acid in acetonitrile.

The mass spectrometer was used in positive ionization mode with nanospray voltage set at 2.4 kV and source temperature at 275°C. Data-dependent acquisition (DDA) mode was used with full MS scans detected in the Orbitrap mass analyzer at a resolution of 120,000. In each cycle of DDA analysis after each survey scan, the most intense ions showing a threshold ion count over 10000 were selected for fragmentation. The number of selected precursor ions for fragmentation was determined by the "Top Speed" acquisition algorithm and a dynamic exclusion of 60 seconds. Fragment ion spectra were generated via high-energy collision dissociation (HCD) at normalized collision energy of 28%. To assess the instrument performance and avoid carryover, digested bovine serum albumin (New England Biolabs) was analyzed between each sample.

Data analysis. To identify tmRNA-tagged peptides we used two complementary analyses. In a first analysis, acquired spectra were analyzed with the denovo and the database search algorithms included in PEAKS Studio software suite (v7.0, Bioinformatics Solutions Inc). For data interpretation we used a customized protein database including a list of common contaminants, all possible *M. pneumoniae* ORFs longer than 19 aa and the ssrAmk tag sequence (87,052 entries). The precursor ion mass tolerance was fixed to 7 ppm, and trypsin was set as enzyme allowing up to three missed cleavages. The fragment ion mass tolerance was set to 0.02 Da for MS2 spectra, and carbamidomethylation on cysteines was set as a fixed modification. Oxidation of methionine and N-terminal protein acetylation were used as variable modifications. False discovery rate (FDR) in peptide identification was set to a maximum of 1% (see Table S6). In a second analysis, acquired spectra were analyzed using the Proteome Discoverer software suite (v2.3, Thermo Fisher Scientific) and the Mascot search engine v2.5 Matrix Science (Perkins et al., 1999). Data searching was performed against a homemade database consisting of all possible truncated proteins containing a ssrAmk tag inserted in each possible position (a total of 239,666 entries, including also the CAT protein, and the ssrA and ssrAmk tag sequences). This database was combined with a list of common contaminants and all possible *M. pneumoniae* ORFs >19aa (87,051 entries). For peptide identification a precursor ion mass tolerance of 7 ppm was used for MS1 level, and trypsin was chosen as enzyme allowing up to three missed cleavages. In this case, the fragment ion mass tolerance was adjusted to 0.5 Da for MS2 spectra, with carbamidomethylation on cysteines set as a fixed modification. Oxidation of methionine and N-terminal protein acetylation were considered as variable modifications. False discovery rate (FDR) in peptide identification was set to a maximum of 5%, and only unique tagged peptides with an ion score >20 were considered. All tagged peptides identified under this criterion were also significant at a more strict filter of 1% FDR (see Table S7). Quality of the mass spectra corresponding to the tagged peptides identified by both pipelines were further validated manually and by using the deep-learning Prosit framework (Gessulat et al., 2019). Comparison of experimental and predicted spectra was assessed by using the Universal Spectrum Explorer (USE) tool (Schmidt et al., 2021).

For the comparative and enrichment analysis after immunoprecipitation under stringent conditions, acquired spectra were analyzed as described above using the Proteome Discoverer software suite (v2.0, Thermo Fisher Scientific) and the Mascot search engine v2.5 Matrix Science (Perkins et al., 1999). In this case, FDR in peptide identification was set to a maximum of 5% and the data were searched against the database containing the list of common contaminants and all possible *M. pneumoniae* ORFs >19 aa (87,051 entries) plus the ssrA and ssrAmk tag sequences (see Table S8). Peptide quantification data were retrieved from the "Precursor ion area detector" node from Proteome Discoverer (v2.0) using 2 ppm mass tolerance for the peptide extracted ion current (XIC). To define putative tagged substrates we established the following criteria and statistical analysis. We followed a peptide-based approach (Burgos et al., 2020) to determine changes in protein abundance between mutant and control IP samples. Two IP mutant/control samples pairs were analyzed independently. Peptides with an ion score lower than 20 were filtered out. Common peptides found in both control and mutant samples were matched by sequence and modifications and the fold change of their quantified areas was computed. Protein fold change was summarized by taking the median value of the fold changes of all peptides of that protein. Putative tagged substrates were identified in each sample pair, as follows: i) differentially detected (DD) substrates were defined as proteins with no peptide detected in the control sample and at least one peptide detected in the mutant sample; ii) differentially enriched (DE) substrates were defined as proteins with a fold change larger than 2. The final list of putative substrates was defined by combining the lists of substrates of the two mutant/control sample pairs as follows: i) DD putative substrate when a protein was a DD substrate in both sample pairs, ii) DE putative substrate when a protein was a DE substrate in both sample pairs. The final protein fold change was computed as the mean of the protein fold changes of the two sample pairs. Candidates were also defined with a more strict filter at 1% FDR (see Table S2).

Immunoblot analysis

Mycoplasma cell lysates were quantified using the Pierce™ BCA Protein Assay Kit. Cell extracts were separated by electrophoresis using NuPage™ 4-12% Bis-Tris polyacrylamide gels (Invitrogen) and proteins transferred onto nitrocellulose membranes using an iBlot™ dry system (Invitrogen). Membranes were blocked in a PBS buffer containing 0.1% Tween 20 supplemented with 5% skim milk (Sigma) or 3% BSA in the case of Strep-tag detection. For immunodetection, membranes were probed with polyclonal anti-CAT (abcam, 1:2,000), monoclonal anti-FLAG M2 (Sigma, 1:5,000), Strep-Tactin conjugated to horseradish peroxidase (IBA lifesciences, 1:10,000), DsRed polyclonal antibody (Takara, 1:2,000), anti-polyclonal

anti-ssrAmk tag (1:2,000) or polyclonal antibodies specific to mycoplasma proteins (kind gift of Dr. Herrmann, Heidelberg University). These include anti-Lon (1:3,000) and anti-FtsH (1:3,000), which were also used as loading controls together with anti-CAT (abcam, 1:2,000) antibody. Anti-mouse IgG (1:10,000) or anti-rabbit IgG (1:5000) conjugated to horseradish peroxidase (Sigma) were used as a secondary antibody. Blots were developed with the Supersignal™ West Femto or West Pico Chemiluminescent Substrate detection Kit (Thermo Scientific) and signals detected in a LAS-3000 Imaging System (Fujifilm).

Expression and purification of strep-tagged proteins

Purification of Strep-tagged proteins expressed in *M. pneumoniae* was performed as follows (Schmidl et al., 2007). Mycoplasma strains were grown in tissue culture flasks containing 20 ml of medium until exponential phase and then splited in triplicate cultures of 60 ml in tissue culture flasks of 300cm^2. Cells were washed twice with binding buffer (100mM Tris-HCl, pH 8; 150mM NaCl) and lysed directly into the flask by scraping off the cells in binding buffer containing 1% Triton X-100 plus protease inhibitor cocktail (Roche). Lysed cells were collected and incubated at 4°C on a rotating platform for 1 h prior centrifugation at 18,000 x g for 10 min. The cell extract supernatant was then applied to a StrepTactin Sepharose High performance column (300 µl bed volume, GE Healthcare) pre-equilibrated with binding buffer at 4°C. After extensive washing with 2.5 volumes of binding buffer, Strep-tagged proteins were eluted with 2.5 mM *d*-Desthiobiotin. Eluted proteins were concentrated in a Vivaspin 500 centrifugal device with a 10 kDa MWCO (Sartorius).

Comparative analysis of relative protein abundances in slow and fast-growing bacteria

For the purpose of the analysis we used proteomic data collected by our group from 7 mycoplasma species exhibiting different growth rates. These include *M. genitalium*, *M. pneumoniae*, *M. capricolum*, *M. mycoides* and *M. gallisepticum* [PXD008243 (Miravet-Verde et al., 2019),], plus two additional protein datasets generated in this study for *M. hyopneumoniae* and *M. feriruminatoris* (see below, PXD025422). In addition, we used available datasets reporting integrated protein abundances for *M. tuberculosis*, *D. vulgaris*, *C. jejuni*, *B. subtilis* [obtained from PaxDB (Wang et al., 2015)] and *E. coli* (Li et al., 2014). The proteome coverage of these datasets is reported in Table S9. For comparison, protein abundances were normalized and represented as relative to all other proteins in the dataset. To estimate the relative abundance of ribosomal protein, we considered the sum of 52 different ribosomal proteins. Student's t-test and Pearson's correlation coefficient were used to evaluate the correlation between protein abundance of specific protein quality control components and bacterial growth rate.

Mass spectrometry analyses of *M. hyopneumoniae* and *M. feriruminatoris*

Sample preparation. Sample preparation for MS analysis of *M. hyopneumoniae* and *M. feriruminatoris* (Jores et al., 2013) were performed as follows. Briefly, 5 ml cultures of *M. hyopneumoniae* or *M. feriruminatoris* were grown for 48 h or overnight, respectively. Cultures were then centrifuged, washed twice in PBS, and the pelleted cells resuspended in 150 µl of urea lysis buffer (6M urea, 0.2M NH_4CO_3) or SDS lysis buffer (4% SDS, 100mM HEPES). Two biological replicates were performed for each condition and bacterial species. Samples were reduced with dithiothreitol, alkylated in the dark with iodoacetamide, digested with LysC/trypsin, and desalted with a MicroSpin C18 column (The Nest Group, Inc) prior to LC-MS/MS analysis (Miravet-Verde et al., 2019).

Mass spectrometry analysis. Samples were analyzed using a LTQ-Orbitrap Velos Pro mass spectrometer (Thermo Fisher Scientific, San Jose, CA, USA) coupled to an EASY-nLC 1000 (Thermo Fisher Scientific (Proxeon), Odense, Denmark). Peptides were loaded onto the 2-cm Nano Trap column with an inner diameter of 100 µm packed with C18 particles of 5 µm particle size (Thermo Fisher Scientific) and were separated by reversed-phase chromatography using a 25-cm column with an inner diameter of 75 µm, packed with 1.9 µm C18 particles (Nikkyo Technos Co., Ltd. Japan). Chromatographic gradients were performed as follows. First at 93% buffer A and 7% buffer B with a flow rate of 250 nl/min for 5 minutes and then gradually increased 65% buffer A and 35% buffer B in 120 min. The column was washed for 15 min with 10% buffer A and 90% buffer B after each analysis. Buffer A: 0.1% formic acid in water. Buffer B: 0.1% formic acid in acetonitrile.

The mass spectrometer was used in positive ionization mode with nanospray voltage set at 2.1 kV and source temperature at 300°C. Ultramark 1621 was used for external calibration of the FT mass analyzer prior

the analyses. Internal calibration was carried out using the background polysiloxane ion signal at m/z 445.1200. The acquisition was done in data-dependent acquisition (DDA) mode and full MS scans with 1 micro scans at resolution of 60,000 were used over a mass range of m/z 350-2000 with detection in the Orbitrap. Auto gain control (AGC) was fixed to $1x10^6$, dynamic exclusion (60 seconds) and charge state filtering disqualifying singly charged peptides was activated. In each cycle of DDA analysis after each survey scan, the top twenty most intense ions with multiple charged ions showing a threshold ion count over 5000 were selected for fragmentation. Fragment ion spectra were generated via collision-induced dissociation (CID) at normalized collision energy of 35% and they were acquired in the ion trap mass analyzer. AGC was set to $1x10^4$, isolation window of 2.0 m/z, an activation time of 10 ms and a maximum injection time of 100 ms were used. All data were acquired with Xcalibur software v2.2. To avoid sample carryover and to assure stability of the instrument, digested bovine serum albumin (New england biolabs) was analyzed between each sample. QCloud (Chiva et al., 2018) was used to control instrument longitudinal performance during the project.

Data analysis. Acquired spectra were analyzed using the Proteome Discoverer software suite (v2.0, Thermo Fisher Scientific) and the Mascot search engine (v2.6, Matrix Science (Perkins et al., 1999)). The data were searched against databases for *M. hyopneumoniae* 232 (94,848 entries) or *M. feriruminatoris* G5847 (75,500 entries) that includes a list (Beer et al., 2017) of common contaminants and all the corresponding decoy entries. For peptide identification a precursor ion mass tolerance of 7 ppm was used for MS1 level, and trypsin was chosen as enzyme allowing up to three missed cleavages. The fragment ion mass tolerance was adjusted to 0.5 Da for MS2 spectra. Carbamidomethylation on cysteines was set as a fixed modification. Oxidation of methionine and N-terminal protein acetylation were considered as variable modifications. FDR in peptide identification was set to a maximum of 5%. Peptide quantification data were retrieved from the "Precursor ion area detector" node from Proteome Discoverer (v2.0) using 2 ppm mass tolerance for the peptide extracted ion current (XIC). The obtained values were used to calculate the protein top 3 area using only unique peptides for protein ungrouped (Table S10).

QUANTIFICATION AND STATISTICAL ANALYSIS

Sample sizes and statistical analysis are detailed for each experimental analysis in methods and their corresponding figure legends. Briefly, RNA differential expression analysis was performed using edgeR v. 3.26.8 (Robinson and Smyth, 2007, 2008; Robinson and Oshlack, 2010; Robinson et al., 2010), using trimmed mean of *M*-values (TMM) normalization, and classical pair-wise comparison. Quantile-adjusted conditional maximum-likelihood (qCML) method was used to test significance of fold changes. Multiple tests correction was applied using Benjamini–Hochberg method (Benjamini and Hochberg, 1995), and fold changes with a corrected *q*-value smaller than 0.05 were considered significant (5% FDR). For mass spectrometry data we used the Mascot search engine and PEAKS Studio software considering 5% and 1% FDR, respectively. Additionally, tagged peptides identified by Mascot were considered significant at 1% FDR. Student's t-test and Pearson's correlation coefficient were used to evaluate the correlation between protein abundance of specific protein quality control components and bacterial growth rate. p values are shown on the figure as *asterisks*: *, $P < 0.05$; **, $P < 0.01$; ***, $P < 0.005$.